



HAL
open science

Recent Relative Sea-Level Changes Recorded by Coral Microatolls in Southern Ryukyus Islands, Japan: Implication for the Seismic Cycle of the Megathrust

S. Debaecker, N. Feuillet, K. Satake, K. Sowa, M. Yamada, A. Watanabe, A. Saiki, J. -M. Saurel, M. Nakamura, G. Occhipinti, et al.

► To cite this version:

S. Debaecker, N. Feuillet, K. Satake, K. Sowa, M. Yamada, et al.. Recent Relative Sea-Level Changes Recorded by Coral Microatolls in Southern Ryukyus Islands, Japan: Implication for the Seismic Cycle of the Megathrust. *Geochemistry, Geophysics, Geosystems*, 2023, 24, 10.1029/2022GC010587 . insu-04155702

HAL Id: insu-04155702

<https://insu.hal.science/insu-04155702v1>

Submitted on 7 Jul 2023

HAL is a multi-disciplinary open access archive for the deposit and dissemination of scientific research documents, whether they are published or not. The documents may come from teaching and research institutions in France or abroad, or from public or private research centers.

L'archive ouverte pluridisciplinaire **HAL**, est destinée au dépôt et à la diffusion de documents scientifiques de niveau recherche, publiés ou non, émanant des établissements d'enseignement et de recherche français ou étrangers, des laboratoires publics ou privés.



Distributed under a Creative Commons Attribution - NonCommercial - NoDerivatives 4.0 International License

Geochemistry, Geophysics, Geosystems[®]



RESEARCH ARTICLE

10.1029/2022GC010587

[†]Deceased 23 December 2021.

Key Points:

- We document relative sea-level history in the southern Ryukyus from modern coral microatoll records
- Interseismic uplift rates indicate a coupling of up to 40% of the deep portion of the megathrust up to 40 km
- We evidenced possible decadal- and decametric-scale slow-slip events below the seismogenic part of the megathrust

Supporting Information:

Supporting Information may be found in the online version of this article.

Correspondence to:




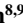

S. Debaecker,
debaecker.sophie@gmail.com

Citation:

Debaecker, S., Feuillet, N., Satake, K., Sowa, K., Yamada, M., Watanabe, A., et al. (2023). Recent relative sea-level changes recorded by coral microatolls in Southern Ryukyus islands, Japan: Implication for the seismic cycle of the megathrust. *Geochemistry, Geophysics, Geosystems*, 24, e2022GC010587. <https://doi.org/10.1029/2022GC010587>

Received 22 JUN 2022
Accepted 19 DEC 2022

Recent Relative Sea-Level Changes Recorded by Coral Microatolls in Southern Ryukyus Islands, Japan: Implication for the Seismic Cycle of the Megathrust

S. Debaecker^{1,2} , N. Feuillet¹, K. Satake³ , K. Sowa^{4,5} , M. Yamada^{3,6}, A. Watanabe³, A. Saiki³, J.-M. Saurel¹, M. Nakamura⁷ , G. Occhipinti^{1,†}, T.-L. Yu^{8,9}, and C.-C. Shen^{8,9} 

¹Institut de Physique du Globe de Paris, Université Paris Cité, Paris, France, ²Now at UMR 7266 LIENSs, CNRS-Université de La Rochelle, La Rochelle, France, ³Earthquake Research Institute, The University of Tokyo, Tokyo, Japan, ⁴Japan Agency for Marine-Earth Science and Technology, Yokosuka, Japan, ⁵Now at KIKAI Institute for Coral Reef Sciences, Kikai, Japan, ⁶Now at Shinshu University, Matsumoto, Japan, ⁷Ryukyus University, Nishihara, Japan, ⁸National Taiwan University, High-Precision Mass Spectrometry and Environment Change Laboratory (HISPEC), Taipei, Taiwan ROC, ⁹National Taiwan University, Research Center for Future Earth, Taipei, Taiwan ROC

Abstract The seismic hazard related to megathrust earthquakes in the Ryukyus (southern Japan) is poorly constrained as no large earthquake has been reported there. The Meiwa tsunami impacted the coasts of the Yaeyama and Miyako islands in 1771 but its origin is still debated. Global Navigation Satellite Systems measurements indicate that strain is accumulating along the plate interface but the observation period is short. It is thus crucial to gain information on the seismic potential of the megathrust. The islands of the Ryukyu archipelago are located in a tropical region and surrounded by reefs where numerous microatolls are growing. They preserved the record of variations of the relative sea-level in their skeleton. We mapped seven sites over five islands and subsequently selected and sampled eight slabs of modern microatolls. The corals have emerged slowly at a rate of 0.7–2.8 mm/yr due to the long-term interseismic loading on the megathrust up to 40 km in deep. The coupling rate estimated from elastic back-slip models ranges between 10% and 100%. We also identified multi-decadal relative sea-level changes of a few cm/yr, likely due to very long duration slow-slip events (SSE) along the shallow or deep parts of the megathrust. Those SSEs occur each 10–40 years and have accommodated 50% of the convergence rate in the last 250 years. Our study provides new constraints on the seismic cycle of the Ryukyu megathrust and on the seismic hazard in this region and suggests that a large megathrust earthquake could occur in the area in the future.

Plain Language Summary We aim to better constrain the seismic and tsunamigenic hazard related to large subduction earthquakes in the Ryukyu archipelago (southern Japan). The behavior (seismic vs. aseismic) of this subduction zone is still debated and we do not know if it has the capacity to rupture during a large thrust earthquake in the future. This is mainly because the historical catalog of seismic events is very short (only few centuries) in this area. Our goal was to find geological markers able to preserve, over several decades or centuries, the trace of past vertical surface deformations of the upper plate above the megathrust. Those deformations are controlled by deep processes along the megathrust, either due to interseismic strain accumulation in between earthquakes or release during the earthquake (coseismic slip). To this goal, we sampled massive corals that are able to record centimetric variations of the sea-level. All corals have emerged at a rate of 2 mm/yr because the plate interface is locked and accumulates strain that may be released in a future large earthquake. We also show that long-duration transient slow-slip events likely occur along the shallower portion of the megathrust. Our study provides new constraints on the seismic hazard in this area.

1. Introduction

The plate interface of a subduction zone can be locked and accumulate strain over decades, centuries and millennia in the interseismic period. During an earthquake this strain is suddenly released (Chlieh et al., 2007; Ozawa et al., 2012; Vigny et al., 2011). This promotes vertical deformations of various signs, rates, and durations at the surface of the overriding plate above the megathrust. Those deformations are controlled by tectonic motions along different portions of the subduction interface during the seismic cycles (coseismic slip, aseismic slip, transient events...). During the last two decades, such deformations were captured by geodetic data along many subduction zones, which has allowed to document and characterize various stages of the seismic cycle (coseismic

© 2023 The Authors.

This is an open access article under the terms of the [Creative Commons Attribution-NonCommercial License](https://creativecommons.org/licenses/by-nc/4.0/), which permits use, distribution and reproduction in any medium, provided the original work is properly cited and is not used for commercial purposes.

and post-seismic motions, interseismic strain accumulation, slow slip events (SSE), Chlieh et al., 2007; Mallick et al., 2021; Meltzner et al., 2015). Geological markers such as marine terraces have also been used to document longer-term deformations accumulated over many seismic cycles (Leclerc & Feuillet, 2019; Taylor et al., 2005) whereas biological markers such as algae or corals are useful to estimate the coseismic vertical motion along the coast after megathrust earthquakes (Meltzner et al., 2006; Reid et al., 2020; Taylor et al., 2008 and references therein). The coupling rate, the geometry and segmentation of the megathrust as well as the recurrence of past earthquakes are critical parameters on which information is needed to better constrain the seismic hazard. This can be achieved by documenting the vertical surface deformation of the overriding plate. During an earthquake, the upper plate is uplifted above the rupture zone and subsides beyond. The transition between uplift and subsidence (hinge-line), where no deformation occurs, roughly corresponds to the downdip limit of the rupture. During the interseismic period, when the stress is recovering, deformations are of strictly opposite signs (Mouslopoulou et al., 2016). When the mechanical behavior of the overriding plate is purely elastic, the stress accumulation and release compensate over one or several seismic cycles and no long-term topography is created. Depending on the mechanical conditions of the plate interface, classical models of the seismic cycle are of three types: characteristic (same magnitude earthquakes occurring at the same time interval), time-predictable (the maximum shear stress at initiation is always the same), or slip-predictable (the shear stress at which the slip ceases has always the same value) (Shimazaki & Nakata, 1980).

Recently, studies have introduced further complexity to these models, by showing that the interseismic strain could vary through time (Mallick et al., 2021; Meltzner et al., 2015), or that megathrust earthquakes could be clustered in time (Mouslopoulou et al., 2016), for example. Furthermore, the recent discovery of non-seismic slip events (SSEs, Very Low Frequency Earthquakes (VLFE), tremors) also questioned the classical models and raised issues for the interpretation of the seismic behavior of subduction zones. It was recently discovered that these slow-slip or transient events may last for decades (Mallick et al., 2021; Meltzner et al., 2015; Weil-Accardo, Feuillet, Jacques, Deschamps, Beauducel, et al., 2016; Weil-Accardo et al., 2020) and consequently may bias our interpretation of the seismic cycle and our estimate of the seismic coupling. This is particularly true when the time scale of observation is too short, which is always the case when only geodetic data are used (Philibosian et al., 2022). As exemplified by the 2004 Sumatra-Andaman and 2011 Tohoku earthquakes, the classical models of seismic cycles, established with short-term data, may fail to predict the occurrence of large earthquakes along many subduction zones worldwide. We thus need to enlarge the time scale of observation by using natural markers able to record the vertical deformations of the overriding plate at time scales of one or several seismic cycles.

One of the main markers available to this goal are coral microatolls in tropical areas (Philibosian et al., 2017, 2022; Sieh et al., 2008; Weil-Accardo et al., 2020). We focused our study at the Ryukyu subduction zone for two reasons (Figure 1). First, the seismic behavior of this subduction zone is poorly known and strongly debated. The coupling estimated from GPS data and moment tensor data of shallow earthquakes is very low (Watanabe & Tabei, 2004), implying that this subduction zone is mostly creeping and cannot promote large earthquakes. However, a giant tsunami, the Meiwa event, was reported in 1771, and many older Holocene tsunami deposits (blocks and sediments) have been documented (K. Goto, Kawana, & Imamura, 2010). Second, many sites where dozens of coral microatolls are growing were recently discovered in several islands of the Ryukyus (Weil-Accardo et al., 2020).

These microatolls are able to record with a centimetric precision the decadal-scale tectonic deformation related to the different periods of the seismic cycle (Weil-Accardo et al., 2020). This opens numerous perspectives both to progress in our understanding of the seismic cycle at subduction zones that are usually considered aseismic, but also to better constrain the seismic hazard related to large thrust earthquakes in the Ryukyus.

We targeted the southern Ryukyu islands where the 1771 Meiwa event occurred and where the inferred seismic coupling estimated from GPS survey and paleotsunamis studies is one of the highest in the arc (5%–35%, Watanabe & Tabei, 2004; 20%, Ando et al., 2018). Fossil coral colonies and microatolls were documented and studied in the area (e.g., Sowa et al., 2014; Yamaguchi, 2016; Yamano et al., 2019) but never for modern tectonic purposes.

During several field trips conducted for reconnaissance and sampling, we discovered many new sites where microatolls are developing in the fringing reefs of the Iriomote, Hateruma, Ishigaki, and Miyako islands. We first present the sites and their geodynamic context, and the methodology we used to sample, analyze and interpret the slices of microatolls we collected. We then describe the corals' stratigraphy and discuss the origin of sea-level variations. We combine local GPS and tide gauge data to obtain an approximate absolute sea-level trend and we

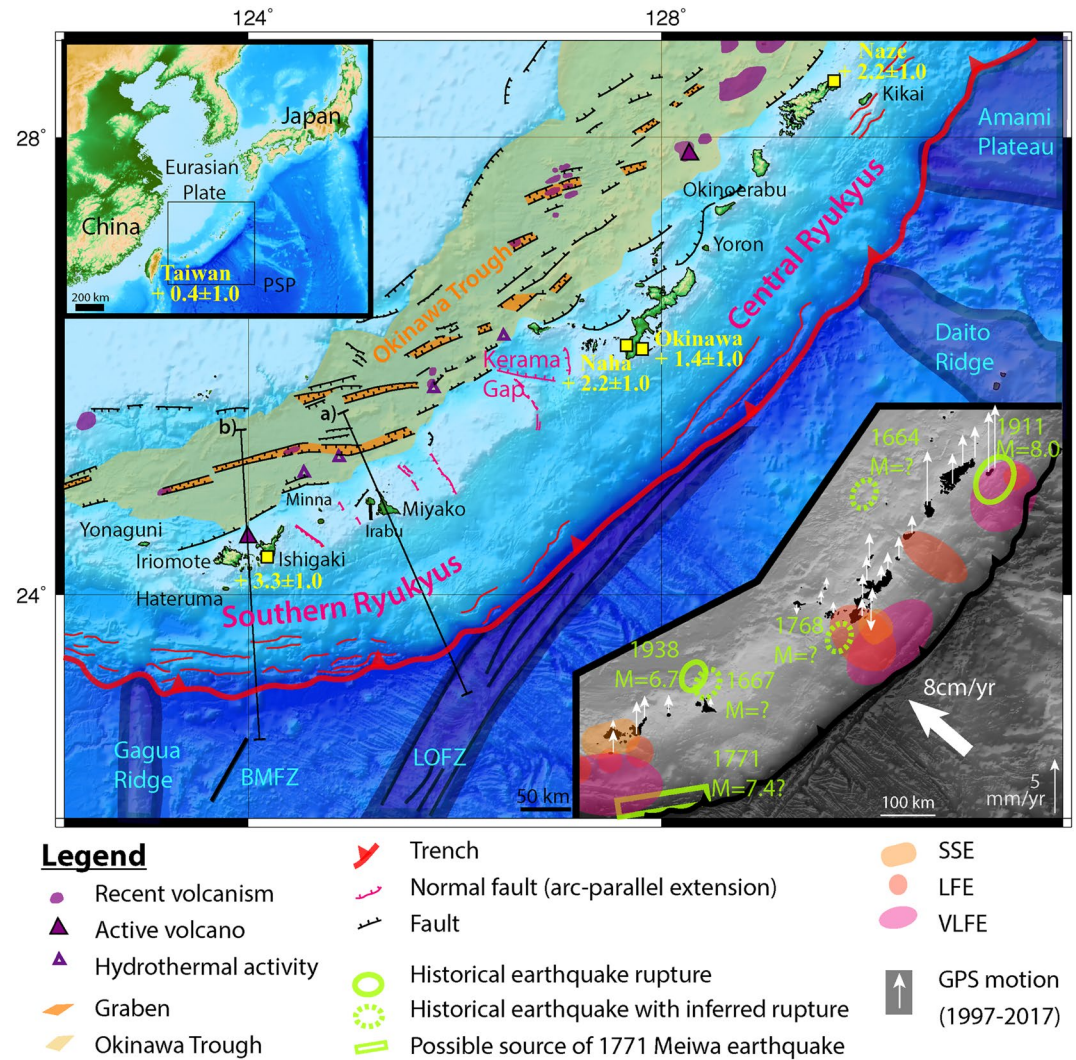


Figure 1. Geodynamic setting of the Ryukyu archipelago. Inset map: Location of the Ryukyu archipelago. PSP = Philippine Sea Plate. Main figure: Tectonic setting in the Ryukyus. Orange area: Okinawa Trough, with volcanic activity in violet and grabens in darker orange. Normal faults related to the arc-parallel extension are indicated in pink color. Accretionary wedge front and splay faults are indicated in red color. Dark blue areas: bathymetric asperities in the subducting plate. LOFZ = Luzon-Okinawa Fracture Zone. BMFZ = Bonin-Mariannes Fracture Zone. Faults are modified after Sibuet et al. (1998), S.-K. Hsu et al. (2013), Minami and Ohara (2018), and H. Goto et al. (2018). Information on hydrothermal activity (open and purple triangles) is from Minami and Ohara (2018). Yellow squares: tide gauge stations for Permanent Service for Mean Sea-Level with mean value of the sea-level rise estimated over the past 40 years. Black lines: location of the cross-sections shown in Figures 2, 13, and 14. Inset: Distribution of historical large-magnitude earthquakes in the Ryukyu islands. White arrows: vertical GPS motion between 1997 and 2017 from Geospatial Information Authority of Japan. Low Frequency Earthquakes and Very Low Frequency Earthquakes are from Nakamura (2017). Slow-slip events are from Nishimura (2014). Hypothetic location of the 1771 Meiwa earthquake source is from Nakamura (2009). Historical earthquakes are from Nakata and Kawana (1995). Convergence rate of the Philippine Sea Plate is from Ando et al. (2009).

compare it with satellite altimetry. We compare the inferred tectonic signal recorded by microatolls with that of the GPS. We model the sea-level variations using elastic models and discuss their origin, the behavior of this subduction zone, and possible implications for the seismic hazard in the Southern Ryukyus.

2. Tectonic and Geodynamic Context of the Ryukyu Subduction Zone

The Ryukyu archipelago is located between the main island of Japan and Taiwan. It results from the subduction of the Philippine Sea Plate (PSP) under the Eurasian plate at a rate of 8 cm/yr (Ando et al., 2009). It is divided

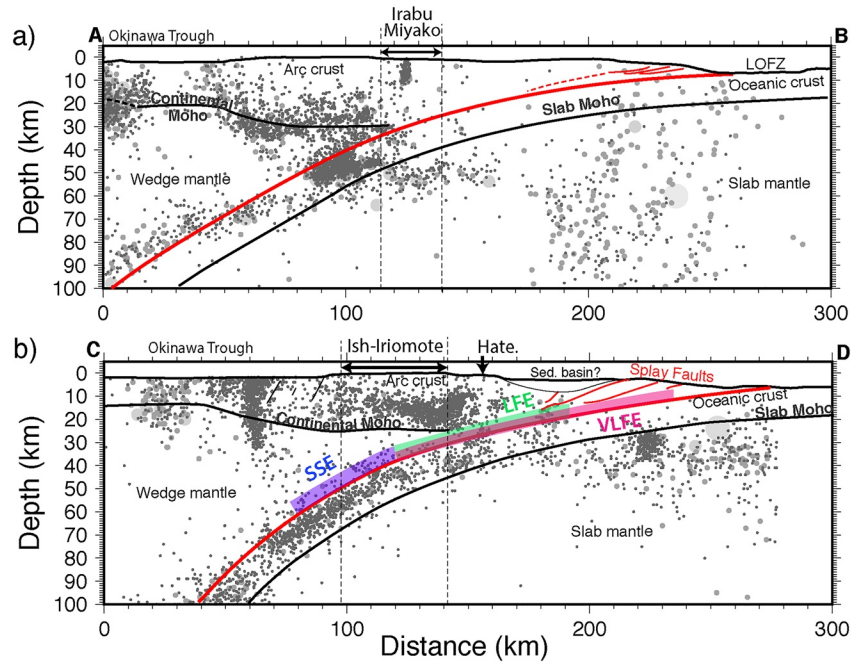


Figure 2. Interpretation of cross-sections of the megathrust around (a) Ishigaki and (b) Miyako. See location of cross-sections in Figure 1. Position of the continental Moho, the slab and the splay faults are inferred from Nishizawa et al. (2017), R. Arai et al. (2016), S.-K. Hsu et al. (2013), Doo et al. (2018) and SLAB 2.0 model (Hayes et al., 2018). Gray dots are seismicity (with magnitude ranging between 3 and 6) from Japan Meteorological Agency from 1980 to 2020. Location of slow-slip events, Low Frequency Earthquakes, and Very Low Frequency Earthquakes, from Nishimura (2014) and Nakamura (2017), is indicated on panel (b). Ish = Ishigaki; Hate = Hateruma; and LOFZ = Luzon Okinawa Fracture Zone.

into three zones: the northern, central, and southern Ryukyus. In the back-arc region, the Okinawa trough opens at rate of 5 cm/yr (Nishimura et al., 2004; Figure 1). There is no clear evidence of a volcanic front in the central or southern Ryukyus (Minami & Ohara, 2018; Shiono et al., 1980). The trench is curved and the subduction becomes oblique west of 126°E in front of the southern Ryukyus (Yaeyama, i.e., Yonaguni, Iriomote, Hateruma and Ishigaki islands, and Miyako islands). In this area, large bathymetric reliefs such as the Gagua Ridge enter the subduction zone and may modify locally the mechanical properties of the plate interface (Cloos, 1992; Dominguez et al., 1998; Y.-J. Hsu et al., 2012), and the coupling rate (Nakamura, 2017; Okamura et al., 2017). This was documented off the southeast coast of Okinawa, where the Luzon Okinawa Fracture Zone enters the subduction system (Tadokoro et al., 2018). The southern Ryukyus are the islands closest to the Taiwanese collision zone, in a region of highly oblique convergence of the PSP and Eurasia (Figures 1 and 2).

Below the southern islands, the structure of the Ryukyu subduction zone at depth has been recently imaged with multichannel seismic reflection/refraction surveys and gravity measurements (R. Arai et al., 2016; Doo et al., 2018; S.-K. Hsu et al., 2013; Nishizawa et al., 2017).

Below the Miyako area, the slab angle increases from 0° to 35° with increasing depth (Figure 2a). The slab plunges with a stronger angle 100 km from the trench and reaches a depth of 35–50 km below the Miyako island. Below Ishigaki area, the slab dip increases from 0 at the trench to 15° down to 15 km depth. Below 20 km depth, the slab dip is larger and reaches 30°. The depth of the continental Moho is estimated at about 25–30 km below the islands.

Splay faults were identified and mapped in the wedge all along the southern Ryukyu trench (Figure 2). Thick undeformed forearc basins are also observed southward, bordered by smaller strike-slip faults (Nishizawa et al., 2017).

As in other subduction zones, SSEs were documented at the Ryukyu plate interface (Figures 1 and 2). SSEs are usually classified depending on their duration and nature: long-term SSEs can last around 0.5 years whereas short-term SSEs last several days (Obara & Kato, 2016). Very Low Frequency Earthquakes (VLFE) have dominant frequencies between 10 and 100 s, and Low Frequency Earthquakes and tremors, around 2–8 Hz (Obara &

Kato, 2016; Shelly et al., 2007). In the Ryukyus, clusters of VLFE were observed south of Iriomote, Okinawa, and Kikai Islands (Nakamura & Sunagawa, 2015), below the accretionary wedge or at the plate interface (Ando et al., 2012; Figure 1 inset). Biannual Mw 6-class SSEs inducing a typical uplift motion on the order of several millimeters at the surface of the overriding plate have been observed between 1997 and 2007 at depths ranging between 20 and 40 km beneath Iriomote Island (Heki & Kataoka, 2008; Figure 1 inset). On a larger time window (1997–2013), Nishimura (2014) observed them between 10 and 60 km depth in clusters similar to VLFE, offshore Iriomote, Okinawa, and Kikai Islands. This spatial distribution may be related to the subduction of bathymetric reliefs. The SSE cluster of Kikai is located in front of the subducting Amami plateau, and the cluster of Iriomote may nucleate on an ancient asperity of the subducted slab (Heki & Kataoka, 2008; Nishimura, 2014). The accumulation of slow earthquakes of different time frequencies, at different depths in the same portion of the megathrust led Nakamura (2017) to suggest that deep SSEs could trigger shallower SSEs down dip of areas able to host tsunami earthquakes (Obara & Kato, 2016). Thus, some studies consider that those clusters of slow events could reveal coupled regions, as they redistribute and accumulate stress in surrounding areas (Ando et al., 2012). Other studies however suggest that the occurrence of slow earthquakes indicates a low coupling and that the megathrust is mostly creeping (R. Arai et al., 2016; Nakamura, 2017; Nishizawa et al., 2017).

The seismogenic potential of the Ryukyus subduction zone has been debated for more than 20 years. The low seismic coupling estimated from the seismic moment released over the last century (between 0% and 5%, Peterson & Seno, 1984; Scholz & Campos, 2012), the lack of megathrust earthquakes and the presence of SSEs led some authors to conclude that this subduction zone is aseismic and mostly creeping (Kao et al., 1998; Nishizawa et al., 2017; Wei & Seno, 1998). On the other hand, studies pointed out the structural and seismological similarities between the Ryukyu subduction zone and other fully coupled plate interfaces worldwide (Sumatra and the North-East Japan) (Ando et al., 2012; Hsu & Sibuet, 2005; Lin et al., 2014). Paleoseismological studies based on paleotsunami records inferred a larger coupling rate, up to 20% (Ando et al., 2018). Gravimetric (Doo et al., 2018) or geodetic data (Global Navigation Satellite Systems [GNSS] or acoustic) indicate a strong interplate coupling at least on the shallow portion of the plate interface (Y.-J. Hsu et al., 2012; Tadokoro et al., 2018; Watanabe & Tabei, 2004).

Two major events were reported during the historical period in the Ryukyu: The 25 June 1911 Kikai earthquake, and the 24 April 1771 Meiwa tsunami.

On 25 June 1911, a Mw-8 earthquake occurred offshore Kikai Island, near the trench (Figure 1) and killed 12 people. It generated 3–5 m high tsunami waves in Amami and Kikai, respectively (Tsuji, 1997). Its source is still debated and inferred to be either an intraplate event within the subducted slab (Konishi & Sudo, 1972), or a shallow interplate event (K. Goto et al., 2013).

One of the best known and devastating tsunamis occurred in the southern Ryukyus on 24 April 1771: the Meiwa tsunami. The waves generated during this event were up to 30 m high and hit all islands nearby (Nakata & Kawana, 1995). The tsunami transported blocks as large as houses and carried sediments 1.5 km away from the reef edge and to an altitude of more than 10 m (K. Goto, Kawana, & Imamura, 2010). The event killed at least 12,000 people in the islands. The origin of this event is unknown and still debated but this tsunami is comparable to those having occurred offshore Sumatra or along the coast of Tohoku in 2004 and 2011, respectively. It was proposed that the Meiwa tsunami was promoted by a magnitude 7.4 to 8.0 earthquake that occurred offshore Ishigaki island (Nakata & Kawana, 1995). Later, Nakamura (2009) proposed that a thrust earthquake, more specifically within the subducted sediments beneath the accretionary wedge, promoted the tsunami. Other studies stated a local event associated with a landslide (K. Goto, Kawana, & Imamura, 2010), a normal fault east of Ishigaki (Nakamura, 2006), or collapses in the accretionary wedge (Okamura et al., 2018).

Sedimentological studies of transported boulders and sediments along the coastline reveal five older tsunamis within the last 2,400 years, with a recurrence time ranging between 150 and 400 years, and likely a total of 8 tsunamis in 4,500 years (Araoka et al., 2013). Nakata and Kawana (1995) also identified four sets of tsunami boulders between 2000 years B.P. and 1771 A.D., implying recurrence times of tsunamis of several hundred to one thousand years. Those results are in agreement with those from stratigraphic studies (600 years, Ando et al., 2018).

Although the sources are still widely debated for the 1771 and 1911 events and unknown for older ones, their occurrence challenges our evaluation of the seismic potential of the area and calls for further investigations. The

last events occurred ~110 and 250 years ago. Given the high convergence rate, a significant slip deficit is likely to have been accumulated to date, bringing the megathrust closer to rupture in a future large-magnitude earthquake.

3. Methodology

3.1. The Use of Coral Microatolls

We seek to document past events on the Ryukyu megathrust and characterize its past and current seismic potential using coral microatolls. Modern coral microatolls are ubiquitous in tropical areas in shallow reef flats. During their growth, over decades or centuries depending on the size and age of the colony, they record the relative sea-level (RSL) changes with a centimetric precision. This makes them a first-order tool to link short-term geodetic and longer-term geological observations. The RSL changes may be of tectonic or climatic origin.

Coral microatolls consist of massive coral colonies that develop in intertidal areas. They were first documented by Stoddart and Scoffin (1979), and associated with a discoidal shape and grow underwater.

Their upward growth is limited by the Highest Level of Survival (HLS), the elevation above which the upper part of the coral dies due to prolonged subaerial exposure (Scoffin et al., 1978; Stoddart & Scoffin, 1979; Taylor et al., 1987). The Highest Level of Growth (HLG), a related term, corresponds to the maximum level the coral can reach in one given year, assuming an unrestricted growth (Meltzner et al., 2010). Both HLS and HLG indicate the maximum elevation of the coral at a specific year. However, if the elevation of the HLS gives precise information on the maximum water height, the HLG will only indicate a minimum elevation of the relative sea-level (Meltzner et al., 2010).

Commonly, the HLS is considered to indicate the extreme lowest tide or Extreme Lowest Water (ELW). However, it recently documented that microatolls can survive, during short time lapses, few centimeters to tens of centimeters above the ELW (4 cm: Briggs et al., 2006; 5–10 cm: Weil-Accardo, Feuillet, Jacques, Deschamps, Beauducel, et al., 2016; Weil-Accardo, Feuillet, Jacques, Deschamps, Saurel, et al., 2016; 19±8 cm, Meltzner et al., 2010; tens of centimeter, Weil-Accardo et al., 2020). This variability points out that the link between HLS and ELW is specific to each site (each site having its own tidal characteristics), and to the coral species and colonies.

The RSL variations during the life of a coral colony shape its skeletal morphology (Figure S1.1 in Supporting Information S1). The coral begins to grow radially on the substrate. Once it has reached its HLS, its upper part dies, and its lower submerged part continues to expand below HLS, laterally. If the RSL is stable, the upper part of the coral remains flat. If the sea-level rises, the coral grows in every direction including upon old dead parts and forms a cup-shape morphology. Finally, if the sea-level drops, the coral undergoes a die-down: the emerged part of the coral dies while the lower part grows laterally, leading to a hat-shape morphology. A hat-shaped microatoll indicates a context of relative emergence whereas a cup-shaped microatoll develops in a context of relative submergence (Figure S1.1 in Supporting Information S1).

The succession of rises and falls of the RSL is thus recorded by the coral skeletal morphology. The change of the RSL can be sudden, as during an earthquake for example, or progressive at timescales ranging from few years to several decades. As they grow in the intertidal zone, very close to the sea surface, microatolls are very sensitive to interannual variability of the sea-level changes due to La Nina, El Nino, The Indian Ocean Dipole or North Atlantic Oscillation events at the scale of oceanic basins (Meltzner & Woodroffe, 2015; Taylor et al., 1987; Weil-Accardo et al., 2020; Zachariasen, 1998 and references therein). The small and temporary decreases of the sea-level due to these variations are recorded, over a wide region, in tide gauges and as die-downs of climatic origin in microatolls. They are small (<10 cm of amplitude), short-lived (one to a few years) and are superimposed to the longer-term sea-level variations related to tectonic or climatic changes (Taylor et al., 1987).

Coral microatolls have been used in climate studies to quantify the glacio-isostatic adjustment (Wan et al., 2020; Woodroffe et al., 2012), evaluate the impact of climatic anomalies such as El Nino climatic oscillations (Song et al., 2012; Woodroffe & McLean, 1990), or estimate the Holocene sea-level changes in the South China Sea and offshore Australia (Leonard et al., 2013; Yu et al., 2009). Coral microatolls were also used for tectonic purposes mainly to document the seismic cycle of the megathrust in several subduction zones such as Vanuatu, Indonesia, Myanmar, Lesser Antilles, Central Ryukyus, Japan and in transform zones such as in Haiti (Meltzner et al., 2006, 2010, 2017; Natawidjaja et al., 2006; Philiposian et al., 2012; Shyu et al., 2018; Sieh et al., 2008; Taylor et al., 1980, 1982; Weil-Accardo et al., 2020; Weil-Accardo, Feuillet, Jacques, Deschamps, Beauducel, et al., 2016; Weil-Accardo, Feuillet, Jacques, Deschamps, Saurel, et al., 2016; Zachariasen et al., 1999, 2000).

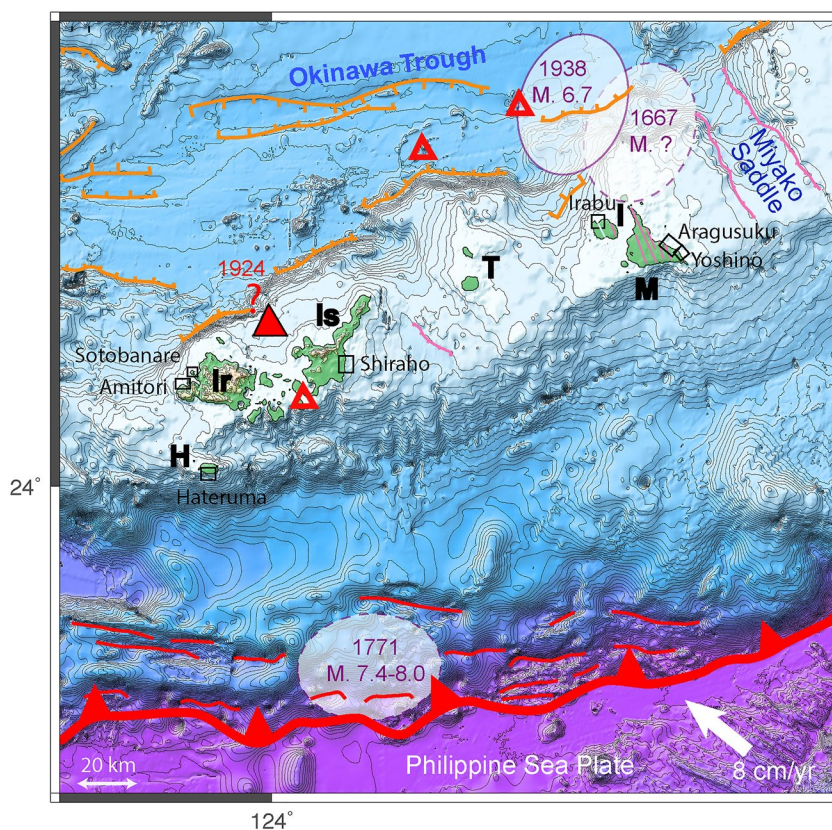


Figure 3. Geodynamical settings of the southern Ryukyus, faults as in Figure 1. White ellipses: rupture areas associated with historical earthquakes inferred from Nakata and Kawana (1995). M = Miyako, I = Iriomote, T = Tarama, Is = Ishigaki, Ir = Iriomote, and H = Hateruma islands. Red filled triangle: possible location of a submarine volcano offshore Iriomote (Kato, 1982). Red open triangles: hydrothermal activity (Minami & Ohara, 2018). Black rectangles are sample locations for this study. Subduction rate is from Ando et al. (2009).

3.2. Survey and Sampling

We performed fieldwork in the islands of Miyako, Ishigaki, Hateruma, and Iriomote between 19 and 29 September 2017, 4–25 July, and 15–24 October 2018 (Figure 3). We identified sites of interest with satellite imagery and photos from Google Earth. We also used drone imagery for the sampling sites of Aragusuku and Yoshino in Miyako Island.

Over 35 sites were investigated. We identified numerous microatolls at six easily accessible sites in four different islands: Miyako (Aragusuku and Yoshino), Ishigaki (Shiraho), Hateruma, and Iriomote (Sotobanare and Amitori) (Figure 3). We checked that every sampling site was connected to the open ocean. Microatolls growing in moated sites, such as pools, cannot be used easily to reconstruct the RSL because they may not record the lower part of the tidal cycle (Smithers & Hopley, 2011).

First, by using a total station, we mapped in detail each site to retrieve, with a precision of a few centimeters, the location and altitude of each microatoll, relative to the total station base. We used the GPS location of the total station and of sampled microatolls with WGS 84 coordinates to obtain its absolute spatial location. We also measured the tide at different times of the day to compare our data with the recorded tide and estimated an absolute value of altitude above the 2018 mean sea-level.

For each microatoll, we measured the external ring (actual HLS for living corals), the center, and when possible, other visible rings and the substrate on which the coral developed (i.e., the base of the coral). The 2018 HLS at the scale of the study area and that of a single microatoll are provided with mean precision of ± 3 and ± 1 cm, respectively. We used the 2018 HLS measurements to select corals whose RSL record would accurately represent the RSL history of the whole study area. Subsequently, we chose the coral to sample under criteria of size (smaller

Table 1
U/Th Dating Results

Sample ID	Weight (g)	²³⁸ U (10 ⁻⁹ g/g) ^a	²³² Th (10 ⁻¹² g/g)	$\delta^{234}\text{U}$ measured ^a	²³⁰ Th/ ²³⁸ U activity ^c	²³⁰ Th/ ²³² Th atomic ($\times 10^{-6}$)	Age (yr ago) uncorrected	Age (yr ago) corrected ^{c,d}	Age (yr BP) relative to 1950 AD	$\delta^{234}\text{U}_{\text{initial}}$ corrected ^b
Hateruma slice	HAT_AI 0.1978	2430.9 ± 2.4	1449.3 ± 3.5	145.0 ± 1.6	0.000591 ± 0.000024	16.4 ± 0.7	56.3 ± 2.3	42.5 ± 7.3	-28.1 ± 7.3	145.0 ± 1.6
	HAT_BI 0.1544	2325.5 ± 3.4	457.8 ± 3.3	143.1 ± 2.3	0.00222 ± 0.000021	185.8 ± 2.2	211.8 ± 2.1	207.3 ± 3.1	138.4 ± 3.1	143.2 ± 2.3
Sotobanara slice	SOTO_B1 0.1974	0.0022 ± 0.0018	3773 ± 10	148.0 ± 1.4	0.001474 ± 0.000058	13.96 ± 0.5	140.1 ± 5.5	100 ± 21	29 ± 21	148.0 ± 1.4
	SOTO_C1 0.2020	2508.5 ± 4.3	132.0 ± 2.3	144.7 ± 3.0	0.001253 ± 0.000025	393 ± 11	119.4 ± 2.4	118.2 ± 2.5	47.6 ± 2.5	144.7 ± 3.0
Irabu slice	IRA_AI 0.2109	2676.1 ± 3.1	151.1 ± 2.2	144.7 ± 1.9	0.001120 ± 0.000016	327.2 ± 6.7	106.7 ± 1.6	105.4 ± 1.7	34.8 ± 1.7	144.7 ± 1.9
	IRA_BI 0.1764	2616.5 ± 2.8	254.6 ± 2.7	145.5 ± 1.8	0.00174 ± 0.00002	295.4 ± 4.4	166.1 ± 1.8	163.8 ± 2.1	94.9 ± 2.1	145.6 ± 1.8
	IRA_C1 0.2019	0.0023 ± 0.0018	134.7 ± 2.3	147.1 ± 1.5	0.002270 ± 0.000016	638 ± 12	216.0 ± 1.5	214.6 ± 1.7	143.9 ± 1.7	147.2 ± 1.5

Note. Analytical errors are 2 sigma of the mean. The different types of police (normal, bold, italic, bold-italic) permitted to indicate in the legend ("d") the date of the chemistry date: HAT_AI, SOTO_C1 and IRA_AI were measured 18 August 2020, HAT_BI was measured 9 December 2018, SOTO_B1 and IRA_BI were measured 25 September 2020 and IRA_C1 were measured 25 November 2018. ^a[²³⁸U] = [²³⁵U] × 137.77 (±0.11%) (Hess et al., 2012); ^bd²³⁴U = (²³⁴U/²³⁸U)_{activity} - 1) × 1000. ^cd²³⁴U_{initial} corrected was calculated based on ²³⁰Th age (T). that is, d²³⁴U_{initial} = d²³⁴U_{measured} × e^(234-λT) and T is corrected age. ^d[²³⁰Th/²³⁸U]_{activity} = 1 - e^{-λ₂₃₀T} / (1 - e^{-λ₂₃₄T}) (Jaffey et al., 1971). ^eAge corrections relative to chemistry date on 18 August 2020, 28 November 2018, 9 December 2018, and on 25 September 2020 were calculated using an estimated atomic ²³⁰Th/²³²Th ratio of 4 (±2) × 10⁻⁶ (Shen et al., 2008).

than the length of the chainsaw) and of apparent history. Further details on coral slices sampling and analysis are presented in Supporting Information S1.

Because of the common occurrence of regrowth colonies above the main coral, RSL changes cannot be accurately retrieved by observing the top surface morphology of a microatoll, and X-ray and/or CT scan images of the coral skeleton are needed (see Supporting Information S1). Uncertainties on our growth band counting are mainly related to the quality of the images we used to interpret the stratigraphy of sampled microatolls. Resolution of CT-scan images is of 1 mm/pixel, and that of the X-ray is of 0.2 mm/pixel. Weil-Accardo (2014) developed a semi-automatic method to identify growth bands on X-Ray imagery. Using uncertainties estimated on both high and low-quality images, a mean uncertainty σ on the growth band counting was defined with the following equation (Weil-Accardo, 2014):

$$\sigma = 0.03 * GB + 0.53$$

with GB being the number of growth bands counted. As we used a combination of X-ray and CT-scan images, we consider that in our study, this method should overestimate error on the growth band counting. Parts of older or fossils corals with complex morphology and gaps in skeletal growth were dated by the U/Th method (see details in Cheng et al. (2000)) to better constrain the chronology of RSL changes. We used a micro core drill device to collect samples by pair along with growth bands in the thin slices. The results of the dating are presented in Table 1. The ages presented in this study are relative to the sampling year of 2018. To reinforce the chronology of the RSL changes and following the methodology applied in other areas (Philibosian et al., 2014), we compared the RSL record of all microatolls and correlated RSL variations (i.e., climatic die downs) with similar age or pattern.

3.3. Analysis of the Coral Skeleton and Reconstruction of the HLS Curves

We counted the high skeletal density bands in the X-Ray image to establish their chronology and we measured their elevations to retrieve the RSL curve between the year of the first HLS and the year of sampling (2018). In the coral stratigraphy, a truncated band marks a HLS, whereas a complete growth band with a flattened highest part corresponds to a HLG (Zachariassen et al., 2000). We plotted the elevation versus ages of all HLS and HLG we identified. The elevation of the youngest 2018 growth band is the reference and is set to 0. From those HLS/HLG curves, we calculated RSL trends by using (a) all HLS (Zach-1, Zachariassen, 1998) (b) all HLG and HLS (Zach-2, Zachariassen et al., 2000) or (c) the first and last HLS only (Zach-3, Zachariassen et al., 2000). We also applied another method proposed by Meltzner et al. (2010) who rather used the highest HLG (as they infer that the HLS impingements during a climatic die-down may be lower than the mean HLS of the coral). As the HLG provides only a minimum estimation of the HLS, Philibosian et al. (2014) suggested discarding the HLG point from the initial growth of the coral, unless its elevation is consistent with the mean trend calculated. For well-constrained records, all methods should produce similar results.

Uncertainties on HLS elevation may be related to erosion of the microatoll, compaction of the substrate, error introduced during fieldwork (i.e., breaks of the coral and measurement) and/or the rescaling and reorientation of the imaged slice. Our microatolls are modern and are located in lagoons; therefore, they are protected from wave erosion and the erosion of their surface is likely minor. During their development, no major earthquake has been reported in the region. For most corals we could reconstruct full images of the slices from both X-Ray and CT-scan. This reduces the uncertainties associated with the imagery process.

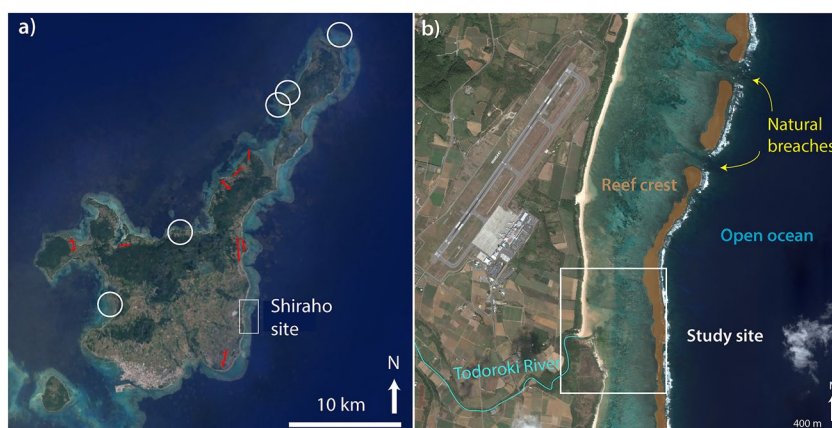


Figure 4. Location of Shiraho study site. (a) Google Earth screenshot. Active faults from Otsubo and Hayashi (2003) are represented as well as the and location of Shiraho site. White circles: other investigated sites. (b) Zoom in the Shiraho area. Natural channels in the reef crest connect the site to the open ocean. White square: study site, see Figure 5.

4. Results

Numerous Porites corals were found in all the islands we visited, with a large variety of colors in tissue (yellow and purple corals were found in Amitori Bay), and shapes: for example, a cup-shaped microatoll was sampled in Aragusuku whereas a hat-shaped coral was found in Irabu (Figure 3). We also found Favia corals in Ishigaki but we focused our study on the Porites species for more consistency between results from different sampling sites.

Those corals developed on the modern reefs which started to develop around 8,000 years ago, after the entry of the Kuroshio Current from the south (Kan, 2011). The warm oceanographic and atmospheric settings induced by the Kuroshio Current, but also the East Asia Monsoon explain the abundance of corals in the reef flats (Denis et al., 2013; Kan, 2011).

We sampled two living corals in Aragusuku site, and one in each following site: Yoshino, Shiraho, Hateruma, Sotobanare, and Amitori (Figure 3). We also sampled one dead microatoll on the island of Irabu near Miyako island.

In the following we present detailed results for one sampling site (Shiraho in Ishigaki). Other sites (Hateruma, Aragusuku, Yoshino, Sotobanare, Amitori, and Irabu) are presented in the Supporting Information S2 in Supporting Information S1. The photographs of the slab, the X-Ray or CT scan, and the interpreted slices with band counting and U/Th ages are presented in Figures S1.3, S1.4, and S1.5 in Supporting Information S1, respectively. We discuss our results on the basis of all the HLS reconstructions that are all presented in the main text.

4.1. The Shiraho Sampling Site

The Ishigaki island is located at 125–160 km distance from the trench. It is 38 km-long and 20 km-wide. The Shiraho reef lies at the south-eastern coast of the island, where the Todoroki River flows into the sea (Figure 4).

The island is surrounded by a fringing reef, composed of a 2 m-deep lagoon and a 150 m-wide reef crest (Figure 4). Although the reef crest emerges during low tide, the area where we found microatoll corals is connected to the open ocean by several natural channels in the north (Figures 4 and 5) and is protected by a fringing reef. Next to the beach, there is an emerged platform, which lies 2 m above the sea-level (green points on Figure 5a). Numerous boulders lie not only on the reef crest but also on the sandy area. Previous research suggested these boulders were transported by a tsunami, triggered by the Meiwa event or older earthquakes (Figure 5a, K. Goto, Miyagi, et al., 2010).

We mapped and measured up to 18 microatolls within the Shiraho study site, which is 550 m-long and 450 m-wide (Figure 5a). The total station was located on the emerged platform. We sampled a 3.9 m-diameter and 50 cm-thick microatoll (SHIR_1_18). Its modern HLS has an average value of -4.72 ± 0.03 m compared to the height of the total station base. This is consistent with the mean modern HLS of the entire site (-4.73 ± 0.06 m), as estimated from the surveyed microatolls height. We consider, thus, this coral to be representative of the entire site.

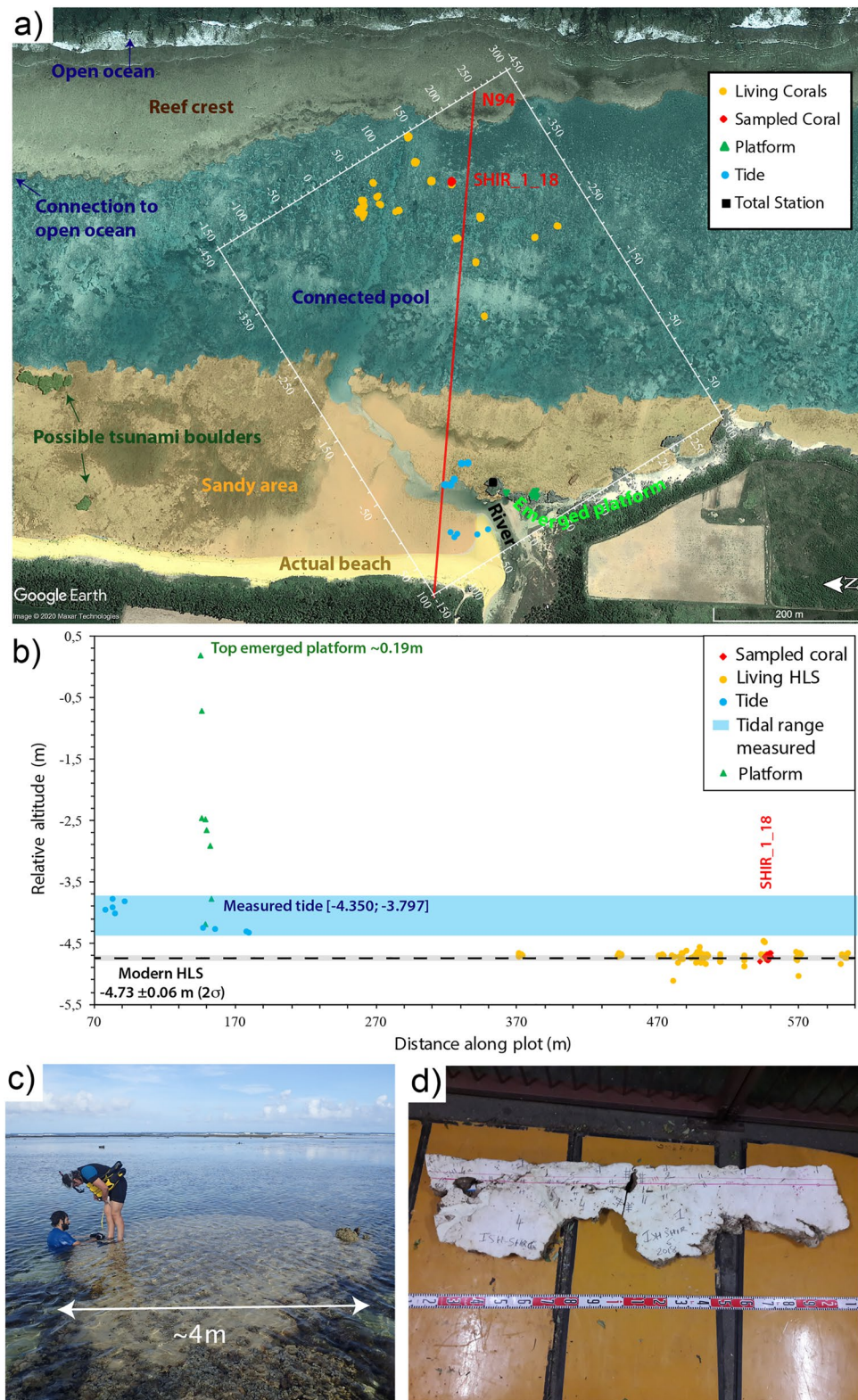


Figure 5.

Table 2

Comparison of the Mean Living Highest Level of Survival of Each Slice With the Extreme Lowest Water of 2018

Island	Site	HLS elevation (cm)	ELW (cm)	Difference (cm)	Evidence for connection to open ocean
Irabu	Irabu	6	-24	30	Yes
Miyako	Yoshino	150	78	72	No
Miyako	Aragusuku	134	78	56	Unclear
Hateruma	Hateruma	50	-23	73	No
Iriomote	Amitori	16	-12	28	Yes
Iriomote	Sotobanare	19	-12	31	Yes
Ishigaki	Shiraho	107	53	54	Yes

Note. The 2018 ELW is estimated from the annual tide gauge records of Ishigaki and Miyako from JODC. For the Irabu, Hateruma, and Iriomote sites, the ELW is estimated from the Ministry of Land, Transport and Infrastructure of Japan (MLIT, https://www1.kaiho.mlit.go.jp/KANKYO/TIDE/tide_pred/7_e.htm).

To compare the altitude of the HLS measurement to the ELW of 2018, we used the tide values recorded during the sampling day by the tide gauge station of Ishigaki (data are available at Japan Oceanographic data center, website jdoss1.jodc.go.jp, black curve on Figure S1.6 in Supporting Information S1).

The HLS is 54 cm above the 2018 ELW (Table 2). This implies that this coral is almost completely emerged for a few hours during the lowest tides of the year (December–February in 2018, Figures S1.7, S1.8, and S1.9 in Supporting Information S1). As there is evidence of the site's connection to the open ocean (Figure 4), we consider here that the tide record of Ishigaki tide gauge station is similar to that of the sampling site. We applied the same protocol to all investigated sites (Table 2).

The microatolls we sampled in Irabu, in Miyako (Aragusuku and Yoshino sites), in Hateruma and in Iriomote (Amitori and Sotobanare sites) islands are 30–73 cm above the 2018 ELW (Table 2). In the Ryukyu islands, the tidal range is about 2 m (Hongo & Kayanne, 2009; Tsuji, 1993; Yamano et al., 2019). Modern HLS, up to 70 cm above the ELW, has been measured in areas with comparable tidal ranges such as Myanmar (Wang et al., 2013), or the Great Barrier Reef (Chappell et al., 1983; Hopley, 1986). This is much higher than in micro-tidal sites (~20 cm, Meltzner et al., 2010). The physiognomy of the sites in Iriomote and Irabu indicates that they are connected

to the open ocean by natural channels in the reef crests (Figures S2.2, S2.5, and S2.11 in Supporting Information S1). It is less clear for the Miyako (Aragusuku and Yoshino, Figure S2.14 in Supporting Information S1) and the Hateruma (Figure S2.8 in Supporting Information S1) sites as the channels are narrower. The difference between the HLS and the 2018 ELW are the highest (up to 73 cm) in the latter sites, indicating that they could be moated.

4.2. Coral Slab Stratigraphy and RSL Record From SHIR_1_18

The 2 m-wide and up to 75 cm-thick slice of the SHIR_1_18 microatoll (Figure S1.3c in Supporting Information S1) and the X-Ray and CT-scan images of its thin slice (Figure S1.4c in Supporting Information S1) reveal a cup-shaped main colony overtopped by regrowth or smaller colonies (Figure 6). The RSL history (Figure 6b) is reconstructed from growth band counting in the X-Ray images (Figure 6a).

The coral started to grow a few years before the first visible band (1897 ± 4) at a rate of 10.0 ± 0.3 mm/yr. It reached its first HLS in 1911 ± 4 , when it experienced its first die-down of 1 cm. In the coral stratigraphy, a small hole of a few centimeters indicates that part of the coral may have been eroded at this place, which is common in the microatolls (Natawidjaja et al., 2004; Suzuki et al., 2008). We use the base of the upper colony to propose a RSL record without the possible erosion (Figure 6). After this first die-down, the microatoll recorded a slight RSL decrease at a rate of 0.3 ± 0.3 mm/yr until 1941 ± 3 . Between 1962 ± 2 and 1998 ± 1 , it recorded a submergence rate of 3.8 ± 0.2 mm/yr, according to the calculation method Zach-2 of Zachariasen et al. (2000) (Table 3). The RSL has been relatively stable ever since.

4.3. Records of Other Corals

Main RSL variations recorded in the slices are summarized in Table 3.

AMIT_1_18 is a 2.5 m-wide and 60 cm-thick cup-shaped microatoll. It was collected on the western side of the Iriomote island (Figures S1.3a, S1.4a, and S1.5a in Supporting Information S1). Several well-preserved rings

Figure 5. Survey in Shiraho. (a) The total station survey points (Main elements of the coastal area: reef crest, platform sandy area...) interpreted from Google Earth image. Red losanges: sampled microatolls; yellow losanges: surveyed corals to estimate the current Highest Level of Survival (HLS). Blue points: tide measurements; green points: relative altitude of the platform. Black square shows the location of the total station. Red line indicates the location of the profile along which each point has been projected. (b) Projection of the HLS measurements with altitude relative to the height of the total station base. (c) Photograph of the in situ microatoll SHIR_1_18. (d) Photograph of the coral slice SHIR_1_18. The pink line drawn on the coral represents the horizontal position of the coral before sampling from the total station measurements.

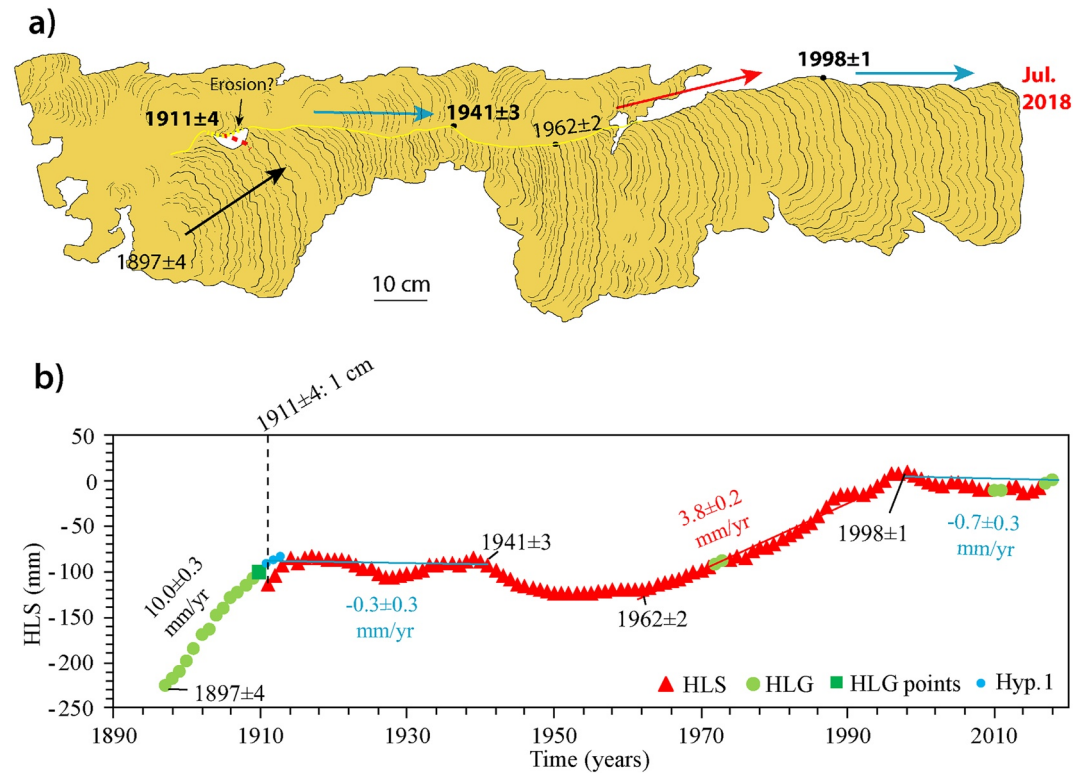


Figure 6. Relative sea-level changes from SHIR_1_18 (Shiraho) stratigraphy. (a) Interpreted slab of SHIR_1_18. Black lines are growth bands, each of them marks 1 year. Thicker black lines are growth bands every 5 years. Black, red, and blue arrows represent the initial growth of the coral, relative submergence, and emergence periods, respectively. Yellow line represents the true Highest Level of Survival (HLS) of the main colony, as it has been preserved from erosion by new growths of other colonies above for at least the last ~25 years. Black dots mark the beginning or end of a relative sea-level (RSL) relative increase or decrease period. (b) HLS variations of SHIR_1_18. Blue and red lines stand for relative emergence and submergence periods respectively, with rate calculated from Zachariassen et al. (2000) using all points from the first HLS. Dashed black line marks the location of a minor die-down of 1 cm in 1911. Date uncertainties reflect growth band counting uncertainty. Other dates show beginning or end of a RSL decrease or increase period. Blue dots are for the hypothesis discussed in the text. Rate in black is the inferred natural growth rate of the coral.

mark its topography (Figure S1.5a in Supporting Information S1). It began to develop in 1927 ± 3 at a growth rate of 8.9 ± 0.3 mm/yr until it recorded a first HLS in 1935 ± 3 . Between 1941 ± 3 and 1951 ± 3 , it recorded a sea-level increase at the rate of 8.2 ± 0.1 mm/yr (Figure 7a). Between 1951 ± 3 and 1976 ± 2 , the microatoll grew in a context of relative sea-level increase at slower rate of 1.3 ± 0.2 mm/yr. Between 1976 ± 2 and 1985 ± 2 the microatoll recorded a sea-level drop by 3–4 cm in two steps. The gap in the coral stratigraphy above those drops could indicate erosion and thus reveal the occurrence of only one drop of at least 7 cm. However such gap was not observed on both sides of the original 10 cm-thick slice (Figure S1.3a in Supporting Information S1). The coral then recorded a sea-level increase that was either sudden or continuous at a rate of 12.0 ± 0.4 mm/yr, higher than the previous coral growth rate. After it reached again the HLS in 1997 ± 1 , the sample reveals two different records of the RSL. First, the main colony showed a main period of RSL increase at the rate of 0.5 ± 1.0 mm/yr between 1997 ± 1 and 2018. This period can be decomposed into a first period of RSL decrease then increase between 1997 ± 1 and 2006 ± 1 , and a second one between 2007 ± 1 and 2018. Such variations were not observed in the coral regrowths 1 and 2 (Figure 7 and Figure S1.5a in Supporting Information S1). The analysis of the regrowth areas 1 and 2 revealed a steady and higher relative sea-level, with a slow increase rate of 0.6 ± 0.6 mm/yr. If this rate is at first order similar to that of the main colony, differences in the RSL elevation or in the variations at the scale of several years could be related to preferential growth toward the center of the coral. As growth bands in the main colony correspond mostly to HLG or eroded HLS annual bands (Figure S1.5a in Supporting Information S1), we will consider records from the regrowths 1 and 2. The AMIT_1_18 microatoll recorded die-downs in 1976 ± 2 and 1980 ± 2 with amplitudes of 3 and 4 cm, respectively. The coral recorded a mean RSL increase at the rate of 1.1 ± 0.2 mm/yr between 1941 ± 3 and 2018.

Table 3
Relative Emergence and Submergence Rates From the Relative Sea-Level Variations Recorded by Our Microatolls Samples

	Zach-1 (all HLS)	Zach-2 (all points)	Zach-3	Corrected rate since 1950
HATE_1_18				
1788–1798		21.6 ± 1.0		
1798–1870	1.5 ± 0.2	1.5 ± 0.2	0.2	
1870–1885	−7.5 ± 0.6	−7.5 ± 0.6	1.1	
1885–1896	–	11.3 ± 0.3	–	
1896–1985	0.3 ± 0.3	0.3 ± 0.2	0.2	2.7 ± 1.2
1998–2018	0.9 ± 0.2	0.9 ± 0.2	0.8	2.1 ± 1.2
SOTO_1_18				
1894–1905	3.0 ± 0.4	3.0 ± 0.4	0.4	
1921–1945	1.3 ± 0.3	1.3 ± 0.3	0.3	
1950–1973	1.7 ± 0.2	1.7 ± 0.2	0.2	1.3 ± 1.2
1986–1997	8.8 ± 1.0	9.1 ± 0.3	0.5	−6.4 ± 1.5
1997–2018	−1.1 ± 0.4	−1.1 ± 0.4	0.4	4.1 ± 1.4
IRA_1_18				
1828–1842	−7.8 ± 1.0	−7.8 ± 1.0	−9.8	
1851–1937	2.8 ± 0.1	3.2 ± 0.2	0.2	
1946–1958	−3.4 ± 0.5	−3.4 ± 0.5	−3.7	6.4 ± 1.9
1986–2014	–	6.8 ± 0.2	–	−4.0 ± 1.3
YOSH_1_18				
1818–1854	–	8.7 ± 0.2	–	
1855–1882	–	9.6 ± 0.2	–	
1882–2018	0.1 ± 0.1	0.1 ± 0.1	0.1	2.9 ± 1.1
ARAG_1_18				
1802–1842		11.1 ± 0.5		
1842–1878	−1.6 ± 0.3	−1.6 ± 0.3	0.3	
1878–1967	0.7 ± 0.2	0.7 ± 0.2	0.2	2.3 ± 1.2
1967–2000	3.4 ± 0.1	3.4 ± 0.1	0.1	−0.4 ± 1.1
2000–2018	0.4 ± 0.5	0.4 ± 0.5	0.5	2.6 ± 1.5
ARAG_2_18				
1810–1840		11.8 ± 0.2		
1862–1876	−0.6 ± 0.3	6.6 ± 0.7	0.7	
1876–1905	4.1 ± 0.4	8.2 ± 0.4	0.9	
1905–2018	2.1 ± 0.1	2.1 ± 0.1	2.1	0.9 ± 1.1
SHIR_1_18				
1897–1911		10.0 ± 0.3		
1917–1941	−0.3 ± 0.3	−0.3 ± 0.3	0.3	
1962–1998	3.8 ± 0.2	3.8 ± 0.2	0.2	−0.8 ± 1.2
1998–2018	−0.9 ± 0.2	−0.7 ± 0.3	0.3	3.7 ± 1.3
AMIT_1_18				
1927–1935		8.9 ± 0.3		
1941–1951	8.2 ± 0.1	8.2 ± 0.1	7.2	
1951–1975	1.3 ± 0.2	1.3 ± 0.2	0.2	1.7 ± 1.2

The SOTO_1_18 coral is a 3 m-long and 70 cm-thick microatoll. It was sampled in Iriomote island, a few kilometers northwards of AMIT_1_18 (Figure S2.1 in Supporting Information S1). The slice is complex and composed of several colonies (Figures S1.3b and S1.4b in Supporting Information S1). The main colony at the base is cup-shaped. We dated two growth bands with the U/Th method to better constrain coral chronology (Figure S1.5b in Supporting Information S1; Table 1). The older, bottom part of the coral could not be analyzed accurately from X-ray or CT-scan imagery, and our RSL record began with the first dated growth band at 1894 ± 4 (Figure 7b). From this date until 1919 ± 4, the coral recorded a sea-level increase of several mm/yr and two large consecutive die-downs of 5 cm in 1916 ± 4 and 1919 ± 4. It then grew in a context of RSL slow increase at a rate of 1.3–1.7 mm/yr until 1973 ± 3. Between 1979 ± 3 and 1986 ± 2, it recorded a die-down of 5 cm in two steps of 2 and 3 cm followed by a rapid sea-level increase. The microatoll reached again the HLS in 1997 ± 2 and recorded a slight decrease of the sea-level at a rate of 1.1 ± 0.4 mm/yr until 2018 (Figure 7b). As it was the case for AMIT_1_18, SOTO_1_18 recorded also small centimetric undulations between 1997 ± 2 and 2018 (Figure S1.5b in Supporting Information S1). The coral recorded die-downs in 1973 ± 3, 1979 ± 3 and 1983 ± 3 with amplitudes of 2, 2, and 3 cm, respectively. The RSL increased at mean rate of 1.7 ± 0.1 mm/yr, between 1894 ± 4 and 2018.

The microatoll HATE_1_18 is ~7 m in diameter. It was collected along the southern coast of Hateruma island (Figure S2.8 in Supporting Information S1). The 4 m-long, 60 cm-thick HATE_1_18 slab (Figure S1.3d in Supporting Information S1) is the longest we collected. It is made of a main central colony A and a smaller external one B. The thick slice (Figure S1.3d in Supporting Information S1) and the CT scan image of the thin slice (Figure S1.4d in Supporting Information S1) revealed a gap of growth between colonies A and B. Counting of growth bands for colony B (Figure S1.5d in Supporting Information S1) indicates that it began to develop in 1998 ± 1. The first growth band of colony B fits the shape of the younger growth band of colony A, which is unexpected. The chronology of RSL changes recorded by colony A was established from U/Th ages obtained on both extremities of the colony and band counting from interpreted CT-Scan images (Figure S1.5d in Supporting Information S1). It died in 1985 ± 2, implying that the coral tissue of the sampling area fully recovered about 10 years after the death of colony A. This is quite unusual. Up to now we cannot explain this recovery and this is beyond the scope of this study. The microatoll HATE_1_18 recorded the RSL changes between 1798 ± 5 and 2018 (Figure 7d). The old colony A began to grow in 1788 ± 5 at high rates of 21.6 ± 1.0 mm/yr. It recorded the first HLS in 1798 ± 5 and grew in a context of slight submergence at the rate of 1.5 ± 0.2 mm/yr until 1870 ± 4. During this period, it shows 6 die-downs occurring every ~8 years in 1803 ± 5, 1813 ± 5, 1825 ± 4, 1839 ± 4, 1849 ± 4, and 1864 ± 4, with an amplitude of 2, 3, 4, 3, 1, and 2 cm, respectively. Between 1870 ± 4 and 1885 ± 4 the coral recorded a sea-level decrease of 11 cm at a rapid mean rate of 7.5 ± 1.1 mm/yr before a sudden or rapid (slower than the natural growth rate of the coral) sea-level increase of the same amplitude. The coral was drowned and caught up again the HLS in 1896 ± 3. It then recorded a slight sea-level increase at the rate of 0.3 ± 0.2 mm/yr until its death in 1985 ± 2. The younger colony recorded a slight sea-level increase at a rate of 0.9 ± 0.2 mm/yr between 1998 ± 1 and 2018. The slab stratigraphy shows several sudden events; one die-down occurred in 1916 ± 3 with an amplitude of 5 cm, which was not

Table 3
Continued

	Zach-1 (all HLS)	Zach-2 (all points)	Zach-3	Corrected rate since 1950
1985–1996	6.6 ± 0.1	12.0 ± 0.4	0.4	−9.3 ± 1.4
1997–2018	0.3 ± 0.1	0.5 ± 1.0	1.0	2.5 ± 2.0
1997–2018 ^a	0.4 ± 0.3	0.6 ± 0.6	0.8	2.4 ± 1.6
1997–2000	−13.8 ± 0.1	−19.3 ± 0.1	−13.8	22.3 ± 1.1
2000–2006	–	8.7 ± 0.1	–	−5.7 ± 1.1
2007–2015	−0.5 ± 0.3	−2.5 ± 0.3	−1.4	5.5 ± 1.3
2015–2018	–	12.7 ± 0.1	–	−9.7 ± 1.1

Note. In column 3, positive and negative values indicate relative submergence and emergence, respectively. We compare Zach_1, Zach-2, and Zach_3 methods (see text). As we do not have enough HLG points in each of those studied periods, we could not use method from Meltzner et al. (2010). All methods give similar results; therefore, we will use the Zach-2 method in our study. The last column shows RSL trend corrected from the absolute sea-level rise of 3 ± 1 mm/yr estimated by Meyssignac and Cazenave (2012) since 1950, on RSL trends for the 1950–2018 time period (see text). Negative and positive trends indicate subsidence and uplift motions, respectively. The bold values indicate natural growth rate of the coral. ^aAMIT_1_18 slice regrowth: RSL records between 1997 and 2018 were recorded both by main colony and regrowth parts. In further analysis, we also consider results from regrowth records.

persistent through time as the HLS retrieved its pre-die-down elevation a few years after. Other main die-downs were documented on colony A in 1947 ± 3, 1954 ± 2, 1970 ± 2, and 1981 ± 2 with amplitudes of 2, 1, 4, and 2 cm, respectively. Between 1800 ± 5 and 2018, HATE_1_18 recorded a mean relative submergence of 0.5 ± 0.1 mm/yr (Figure 7d).

IRA_1_18 is a 4 m-wide fossil coral that was collected in Irabu island, west of Miyako (Figure S2.11 in Supporting Information S1). The RSL record was established by band counting and U/Th age obtained at three growth bands (Table 1, Table S1 and Figure S1.5e in Supporting Information S1). The coral is composed of two colonies: the main colony, colony A, is the largest and the oldest. Colony B is smaller and lower, and it was alive when we sampled it. It started to develop from a small external edge of the colony A after its death. From band counting and U/Th dating (Figure S1.4e in Supporting Information S1), we estimated that colony A started to grow around 1762 ± 5. The orientation of the growth axis and the morphology of the colony indicate that it was overturned. The exact date of its overturning is unclear. The abrupt increase of ~4 cm of the RSL at 1823 ± 3 could indicate that the coral grew upward and that the coral overturned before (Figure S1.5e in Supporting Information S1). We will consider RSL records from 1823 ± 3. Between 1828 ± 3 and 1842 ± 3 the microatoll recorded a rapid sea-level drop of ~13 cm at a rate of 7.8 ± 1.0 mm/yr. After 1842 ± 3, the colony recorded 9 years of RSL stability and sudden or rapid submergence of 11 cm in 1851 ± 3 (Figure 7e). The coral was drowned and reached again the HLS in 1863 ± 3. The microatoll then recorded a period of relative submergence at a rate of 3.2 ± 0.2 mm/yr until 1937 ± 2 and then was almost entirely

killed by a main sea-level drop of at least 19 cm, in 1946 ± 2 years at the latest. It then recorded a stable sea-level in the following 10 years before its death in 1959 ± 2. Less than 30 years later at 1986 ± 2, colony B grew freely at a natural growth rate of 7.8 ± 1.0 mm/yr to reach the HLS in 2014 ± 1 (Table 3). The RSL suddenly dropped by 5 cm at 2014 ± 1. Between 2014 ± 1 and 2018, the coral had been growing freely upward. The main RSL increase trend recorded by IRA_1_18 between 1828 ± 3 and 2018 is of 0.2 ± 0.5 mm/yr.

The microatolls ARAG_1_18 and ARAG_2_18 (6 and 5 m of diameter; 55 and 40 cm-thick, respectively) were both collected in the Aragusuku site along the southeastern coast of Miyako island (Figure S2.14 in Supporting Information S1). ARAG_1_18 is a 3.5 m-long slice (Figure S1.3f in Supporting Information S1). The interpretation and band counting of the CT-scan image of the thin slice (Figure S1.4f in Supporting Information S1) indicate that it began to grow in 1783 ± 8 and was overturned at the beginning of its life, in 1802 ± 7 (Figure S1.5f in Supporting Information S1). We do not present here the overturned part, prior to 1802. It then developed toward the surface at a natural growth rate of 11.1 ± 0.5 mm/yr until it reached its first HLS in 1842 ± 6 (Figure 7f). It recorded a sea-level drop at a rate of −1.6 ± 0.3 mm/yr between 1842 ± 6 and 1878 ± 5, and a sea-level increase at rates ranging between 0.4 ± 0.5 and 3.4 ± 0.1 mm/yr between 1878 ± 5 to 2018.

ARAG_2_18 is a 2.7-m long, up to 70 cm-wide slice (Figure S1.3 g in Supporting Information S1). The interpretation and band counting of the CT-scan image (Figure S1.4g in Supporting Information S1) revealed that it began to grow in 1810 ± 7 at a natural growth rate of 11.8 ± 0.2 mm/yr (Figure 7g). It reached the first HLS between 1845 ± 6 and 1853 ± 6 before recording a large sea-level drop of a minimum of 20 cm (either in one step in 1853 ± 6 or in two steps in 1845 ± 6 and 1853 ± 6, this part being unclear because of possible erosion). The sea-level was stable in the following years, then it increased by 28 cm in the following years in two steps: (a) In the first period between 1862 ± 6 and 1876 ± 5, the sea-level increased at a rate of 6.6 ± 0.7 mm/yr and in 1876 ± 5, the microatoll underwent a die-down of 5 cm. (b) The following years the coral was drowned, either by a sudden or a very rapid (>8.2 ± 0.4 mm/yr) sea-level rise, and grew freely toward the surface to catch up the HLS again in 1905 ± 4.

Although they are very close (130 m apart), ARAG_1_18 and ARAG_2_18 recorded a slightly different history. ARAG_1_18 recorded several die-downs in 1878 ± 5, 1949 ± 3, and 1967 ± 2 with amplitude of 5, 4, and 2 cm, respectively and a mean relative submergence rate of 0.6 ± 0.1 mm/yr between 1842 ± 6 and 2018, and of

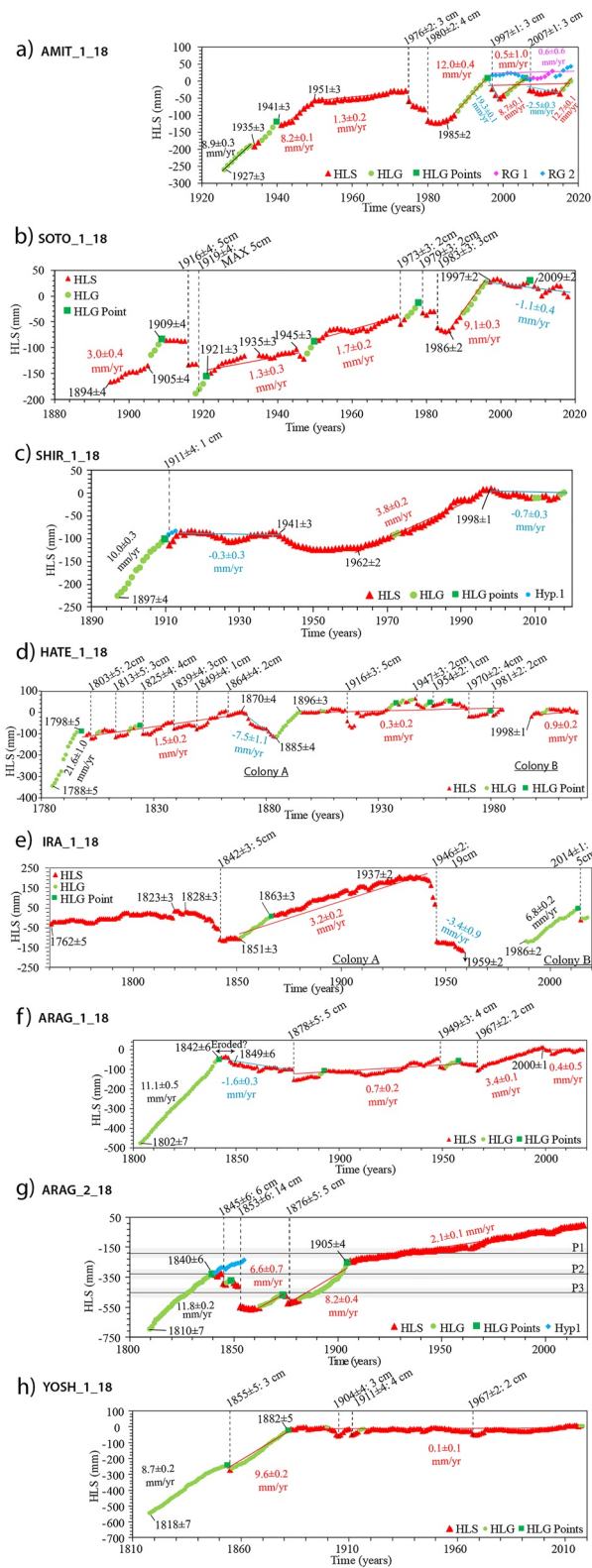


Figure 7.

1.9 ± 0.1 mm/yr between 1967 ± 2 and 2018 (Figure 7f). ARAG_2_18 recorded three die-downs, in 1845 ± 6 , 1853 ± 6 , and 1876 ± 5 with amplitudes of 6, 14, and 5 cm, respectively and a mean relative submergence rate of 2.3 ± 0.5 mm/yr (Figure 7g). Common die-down events may be observed in the mid-19th century (1842 ± 6 being the first HLS for ARAG_1_18) and around 1875–1878.

In the neighborhood of ARAG_1_18 and ARAG_2_18, we measured many other microatolls, some of which were fossils (Figure S2.15 in Supporting Information S1). They are located at three levels (plateaus) P1, P2, P3 at -1.36 ± 0.03 , -1.48 ± 0.03 , -1.60 ± 0.02 m compared to the total station base. Those levels are lower by 19, 33, and 45 cm than the modern HLS (-1.15 ± 0.02 m) and define three older HLS. The lower one P3 is close to the HLS of ARAG_2_18 prior to the 1876 ± 5 die-down. Another plateau P2 could also correspond to the HLS level measured before 1845 ± 6 die-down. However, further analysis of those fossils (including U/Th dating) is necessary to estimate the age of the fossil plateaus.

Those main sea-level drops of the site were not imprinted in the skeleton of ARAG_1_18. The differences in HLS elevation of the two microatolls reached up to 47 cm in 1855 ± 5 then decrease with time to become negligible starting from 1967 ± 2 (Figure S2.15 in Supporting Information S1). This may be because our chronology is not well established (the coral may have begun to record the RSL changes after 1967 ± 2). Another hypothesis may be that before the RSL drops recorded in ARAG_2_18 in 1853 ± 6 , ARAG_1_18 grew in a moated pool and was not able to properly record the sea-level variations. The drone imagery of the site (Figure S2.15 in Supporting Information S1) shows that ARAG_2_18 is located higher on the reef crest whereas ARAG_1_18 is surrounded by many other big microatolls that may have acted as barriers separating ARAG_1_18 from the open ocean during certain periods (see more details in S2 in Supporting Information S1).

The third microatoll we sampled in Miyako, 1.5 km southeastward of the Aragusuku site, is YOSH_1_18. The sampled slab is 2.8 m-long and 80 cm-thick (Figure S1.3h in Supporting Information S1). Interpretation and band counting of the X-Ray (Figures S1.4h and S1.5h in Supporting Information S1) revealed that the coral began to grow in 1818 ± 7 at an averaged growth rate of 8.7 ± 0.2 mm/yr (Figure 7h). It reached a first HLS and recorded a die-down of 5 cm in 1855 ± 5 and then grew upwards in a context of sudden or rapid submergence to reach again a HLS in 1882 ± 5 . It then recorded a roughly stable sea-level (0.1 ± 0.1 mm/yr) until 2018 and small die-downs in 1904 ± 4 , 1911 ± 4 , and 1967 ± 2 , with amplitudes of 3, 4, and 2 cm, respectively. Between 1855 ± 5 and 2018, the coral recorded a stable RSL rate of 0.9 ± 0.1 mm/yr.

The growth rate of the microatolls we sampled ranges between 6.8 ± 0.2 and 21.6 ± 1.0 mm/yr, with an average of $\sim 11 \pm 4$ mm/yr, in agreement with previous estimations for this species in the Ryukyus (5 and 25 mm/yr, Weil-Accardo et al., 2020) and elsewhere (Meltzner & Woodroffe, 2015). It is however slightly higher than other estimates obtained on fossil corals in the Ryukyus (7–10 mm/yr, Suzuki et al., 2008). Microatolls with higher natural growth rates (21.6 ± 3 mm/yr for HATE_1_18) recorded more die-downs than others, in agreement with other studies (Weil-Accardo, Feuillet, Jacques, Deschamps, Beauducel, et al., 2016; Zachariasen et al., 1999, 2000).

5. Discussion

We sampled eight slabs of Porites microatolls that recorded the RSL changes between 1800 and 2018, that is a time-period that spans more than two centuries. All HLS curves are presented together in Figure 8. The microatolls grew in the context of submergence at mean rates ranging between 0.2 ± 0.5 and 2.3 ± 0.5 mm/yr (Figure 8; Table 4). According to criteria developed by Taylor et al. (1987), they all recorded small and temporary climatic die-downs of a few centimeters.

5.1. Comparison Between RSL Records

5.1.1. Decadal Events

In addition to the long-term sea-level variations and temporary small die-downs, all microatolls recorded strong decadal variations of the RSL (either submergence or emergence) with amplitudes of up to ~ 30 cm and durations

Figure 7. Combination of all Highest Level of Survival (HLS) curves of our study. Legend as in Figure 6. HLS curves of (a) AMIT_1_18. Pink and blue points indicate HLS bands interpreted from upper regrowth colonies. (b) SOTO_1_18. Uncertainties prior to 1919 are related to growth band counting and U/Th dating. (c) SHIR_1_18. (d) HATE_1_18. Uncertainties prior to 1985 are related to growth band counting and U/Th dating. (e) IRA_1_18. Uncertainties prior to 1959 are related to growth band counting and U/Th dating. (f) ARAG_1_18. HLS points between 1842 and 1849 may correspond to an eroded part of the coral. (g) ARAG_2_18. Blue points indicate HLS elevation without a possible erosion of the colony. (h) YOSH_1_18.

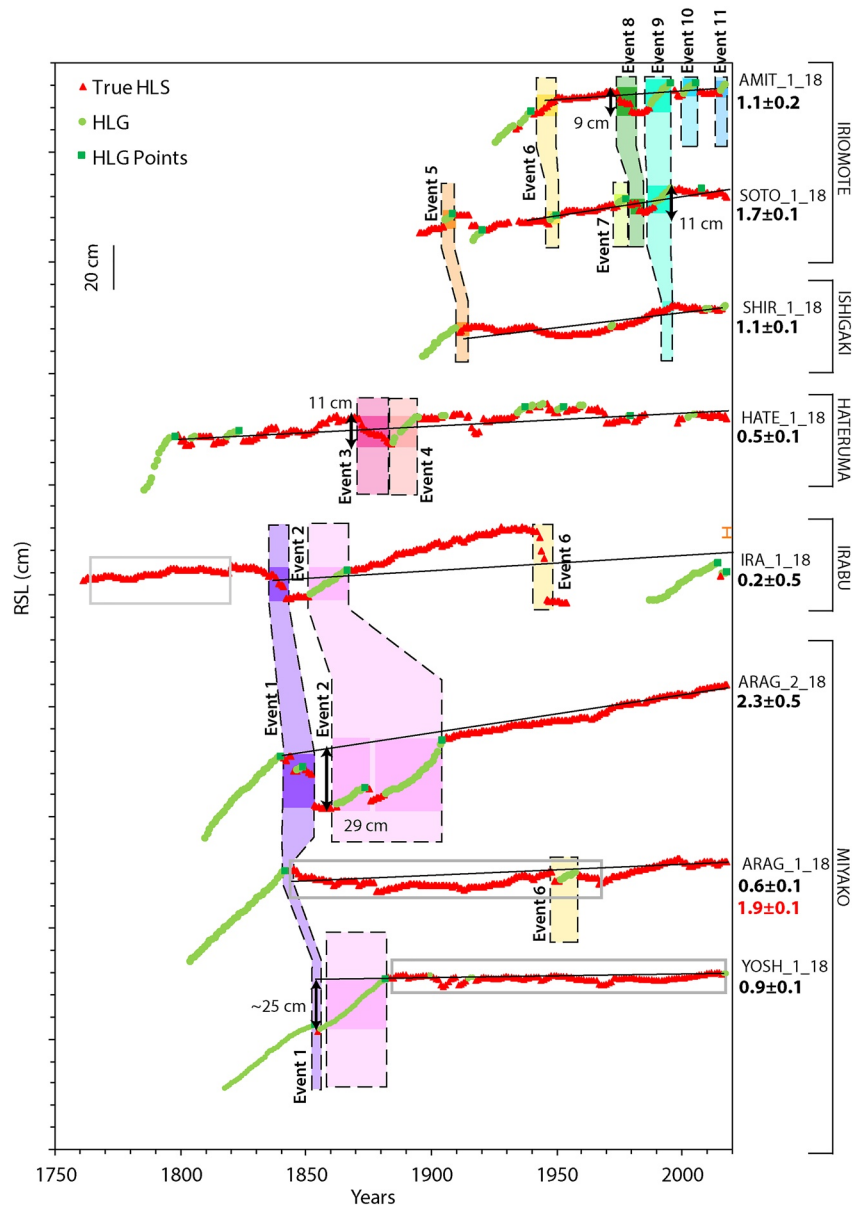


Figure 8. Combination of all Highest Level of Survival curves of our study. We propose here to correlate events identified in the slices. Main events are contoured by bold dashed lines. Maximum duration and amplitude of the events are shown with an opaque rectangle, and the amplitude of main events is shown with double arrows. Light gray rectangles indicate periods of relative sea level (RSL) variations with a specific pattern (e.g., overturning in IRA_1_18, and possible moating in ARAG_1_18 and YOSH_1_18), most of which were not considered in the RSL mean trend estimates. Mean RSL trends are indicated for each microatoll in bold, and another trend has been calculated for ARAG_1_18 since 1967, when the moating effect seems to have been reduced.

ranging between 1 and 42 years. The amplitude for all events is summarized in column 4 of Table 5. These events are numbered between 1 and 11 in Figure 8. Strikingly, they often occur in pairs, following the same pattern: a significant decrease of the sea-level, either in one or two steps, and a consecutive sea-level rise of about the same amplitude during which the microatoll is drowned and grows freely upward to reach the HLS few years or decades later. Those decadal variations do not affect the pattern of longer time scale sea-level records.

In Figure 8, three main pairs of larger events (1/2, 3/4, and 8/9) can be distinguished. The first events 1 and 2 occurred around 1845 and were recorded in Miyako archipelago (in Irabu, Aragusuku, and Yoshino sites). In Aragusuku, ARAG_2_18 recorded a sea-level drop of 21 cm.

Table 4

Relative Submergence Rates in mm/yr With 2σ Uncertainties Estimated From Different Methods Of Zachariasen (1998), Zachariasen et al. (2000), and Meltzner et al. (2010)

Sample	Zach-1 (all HLS)	Zach-2 (all points)	Zach-3	Meltzner	Mean relative submergence	Mean interseismic rate
SHIR_1_18	1.1 ± 0.2	1.1 ± 0.1	1	–	1.1 ± 0.1	1.9 ± 1.1
AMIT_1_18	0.1 ± 0.2	1.2 ± 0.1	0.2	2.1 ± 0.3	1.1 ± 0.2	1.9 ± 1.2
SOTO_1_18	1.5 ± 0.1	1.5 ± 0.1	1.5	2.2 ± 0.2	1.7 ± 0.1	1.3 ± 1.1
HATE_1_18	0.6 ± 0.1	0.6 ± 0.1	0.3	0.7 ± 0.1	0.5 ± 0.1	2.5 ± 1.1
IRA_1_18	0.8 ± 0.3	-0.1 ± 0.1	-0.2	–	0.2 ± 0.5	2.8 ± 1.5
YOSH_1_18	0.2 ± 0.1	0.8 ± 0.1	1.7	–	0.9 ± 0.1	2.1 ± 1.1
ARAG_1_18 ^a	1.8 ± 0.1	1.8 ± 0.1	2.1	–	1.9 ± 0.1	1.1 ± 1.1
ARAG_2_18	2.9 ± 0.1	3.1 ± 0.1	1.8	1.1 ± 0.8	2.3 ± 0.5	0.7 ± 1.5

Note. Rates are calculated on the overall RSL signals recorded by each coral. We averaged value from all methods (column 6) for further discussion. Column 7 indicates interseismic rate obtained after correction of the relative submergence from the absolute sea-level rise of 3 ± 1 mm/yr (Meyssignac & Cazenave, 2012). Positive value corresponds to an uplift motion.

^aIn ARAG_1_18 slice we mostly considered RSL signal after 1967, when the microatoll is the most likely connected to the open ocean.

Table 5

Relative Sea-Level Events Possibly Corresponding to Transient Tectonic Events (Slow Slips at Plate Interface)

Sites	Distance to the trench (km)	Period (years)	Amplitude (cm)	RSL (cm/yr)	Land motion (cm/yr)	Event
ARAG_1_18	147	–	Min 1	–	–	Event 1 (mid-19th century)
ARAG_2_18	147	13	21	-1.6 ±0.1	1.9 ±0.2	
YOSH_1_18	147	–	–	–	–	Event 2 (mid-19th century)
IRA_1_18	166	14	13	-0.8 ±0.1	1.1 ±0.2	
IRA_1_18	166	15	11	0.7 ±0.1	-0.4 ±0.2	
ARAG_2_18	147	42	29	0.7 ±0.1	-0.4 ±0.2	
YOSH_1_18	147	27	25	0.9 ±0.1	-0.6 ±0.2	Event 3 (1870–1985)
HATE_1_18	97	15	11	-0.7 ±0.1	1.0 ±0.2	
HATE_1_18	97	10	11	1.1 ±0.1	-0.8 ±0.2	Event 4 (1885–1900)
SOTO_1_18	134	5	5	1.0 ±0.1	-0.7 ±0.2	Event 5
SHIR_1_18	131	4	2	0.5 ±0.1	-0.2 ±0.2	Event 6 (mid-20th century)
IRA_1_18	166	1	19	-19.0 ±0.0	19.3 ±0.1	
AMIT_1_18	129	9	7	0.8 ±0.1	-0.5 ±0.2	
SOTO_1_18	134	8	6	0.7 ±0.1	-0.4 ±0.2	Event 7
SOTO_1_18	134	6	4	0.6 ±0.1	-0.3 ±0.2	
AMIT_1_18	129	9	9	-1.0 ±0.1	1.3 ±0.2	Event 8 (1975–1985)
SOTO_1_18	134	7	5	-0.7 ±0.1	1.0 ±0.2	Event 9 (1985–1995)
AMIT_1_18	129	11	13	1.2 ±0.1	-0.9 ±0.2	
SOTO_1_18	134	12	11	0.9 ±0.1	-0.6 ±0.2	Event 10
SHIR_1_18	131	7	2	0.3 ±0.1	0.0 ±0.2	
AMIT_1_18	129	7	6	0.9 ±0.1	-0.6 ±0.2	Event 11
AMIT_1_18	129	4	4	1.3 ±0.1	-1.0 ±0.2	

Note. The amplitude of the RSL values is presented in column 4 and their duration in column 3 (see also Figure 9). We deduced the annual RSL trend in cm (column 5, negative values: relative emergence signal, positive value: submergence). The possible land motions by considering a tectonic origin for all events (positive values: uplift, negative value: subsidence) are presented in column 6. The values are corrected from the global sea-level rise value (3 ± 1 mm/yr (i.e., 0.3 ± 0.1 cm/yr, see text)). Indicative age for main events is given in the last column.

Event 2 corresponds to a relative submergence recorded by the microatolls sampled in Aragusuku, Yoshino, and Irabu. Its amplitude varies from 15 cm in Irabu to 30 cm in Aragusuku. In Aragusuku, event 2 occurred in two steps of relative sea-level increase interrupted by a small die-down in 1876 ± 5 .

Events 3/4 were only observed in Hateruma, between 1870 and 1900. It is a 15 years-long RSL drop of 12 cm, immediately followed by an increase of the same duration and amplitude.

Event 6 was recorded in Amitori, Sotobanare, Irabu, and Aragusuku islands. However, it corresponds to a RSL increase of up to 7 cm during less than 10 years, except in Irabu where we observe an abrupt RSL decrease of 19 cm (Table 5). Event 6 may correspond to two synchron events, one corresponding to a RSL increase along the southern Ryukyus, and another one that induced a strong drop of the RSL in Irabu.

Event 8 occurred around 1975–1995 and was recorded in Iriomote at both sites of Amitori and Sotobanare with a maximum amplitude of 12 cm. Shortly after, during event 9 between 1987 and 1996, AMIT_1_18, SOTO_1_18 but also SHIR_1_18 from Ishigaki island recorded a relative sea-level increase (Figure 8). Both corals from Iriomote island reached again the HLS along the mean long-term trend 25 years later in 1996–1997.

Other events are smaller and less clear.

In Aragusuku, we also found dead corals close to the beach (Figure S2.15 in Supporting Information S1). Interestingly, the HLS shown by their topmost part marks coincides with the HLS in the mid-19th century of ARAG_2_18 microatoll. Although we did not estimate the date at which they died, the similar HLS level between fossil corals and growth area in the mid-19th century of ARAG_2_18 microatoll suggest that a catastrophic event may have completely killed many other microatolls in the area. We note that the ARAG_2_18 microatoll recovered the HLS along with the long-term trend, only 60 years later in 1905 ± 4 . Such an event was not observed in ARAG_1_18 microatoll, as it has not recorded the RSL drops of 1845 ± 6 and 1853 ± 6 .

5.1.2. Differences in Die-Downs

In addition to having recorded the same large and long-lasting sea-level variations described above, the microatolls recorded other smaller and shorter-lived events that are more classic climatic die-downs (Meltzner & Woodroffe, 2015; Taylor et al., 1987; Weil-Accardo et al., 2020; Zachariasen, 1998 and references therein; Figure 9).

HATE_1_18 recorded die-downs with a mean recurrence time of 8 years between 1798 ± 5 and 1835 ± 4 . In IRA_1_18, the record older than 1828 was not considered because the growth bands are unclear and the older part of the coral is possibly an overturned colony (Figure S1.5e in Supporting Information S1). Similarly, RSL signals of YOSH_1_18 and of ARAG_1_18 prior to 1967 are surprisingly stable, although their respective RSL signals is affected by several die-downs (see Supporting Information S1). In Figure 9, we documented the main die-downs observed in the slices we sampled. Most die-downs (gray dashed lines in Figure 9) are observed before a gradual increase of the RSL. We also note that those die-downs are also documented in several slices collected in either the Ishigaki or Miyako area, which indicates a regional rather than local process. We note that die-downs associated with the main RSL events identified in Figure 8 (black dashed line in Figure 9) are followed by RSL stability or decrease. Those die-downs define the mid-19th century event, which gathers events 1 and 2 of Figure 8, the mid-20th century event that mostly corresponds to event 6 in Figure 8, and to the 1975/1995 event which coincides with event 8 in Figure 8.

To discuss the origin of the RSL signal in coral microatolls, several criteria were developed by Taylor et al. (1987) and Zachariasen (1998), such as the amplitude and spatial distribution of the RSL event, as well as its co-occurrence with historical earthquake and presence of regrowth afterward. In Figure 10, we summarized the main die-downs we identified in each slice. Die-downs indicated by a gray line are die-downs observed in several sites and/or of amplitude of less than 5 cm, and/or that are followed by a rapid increase of the HLS in the coral stratigraphy. In addition to that information, at the exception of one earthquake of magnitude of 6.7 in 1938, no significant earthquake has been reported in historical time (Figure 1), indicating that the observed die-downs are of climatic origin. At this point of the study, we can not decipher the origin of the larger events associated with the mid-19th century, the 1870/1900, the mid-20th century and the 1975/1995 events (Figures 9 and 10).

Bleaching events, which are common in the southern Ryukyus (Harii et al., 2014), were documented in 1998 and 2003 (Okamoto et al., 2007). Harii et al. (2014) also reported anomalous years in 1983, 1988, 1993, 1998,

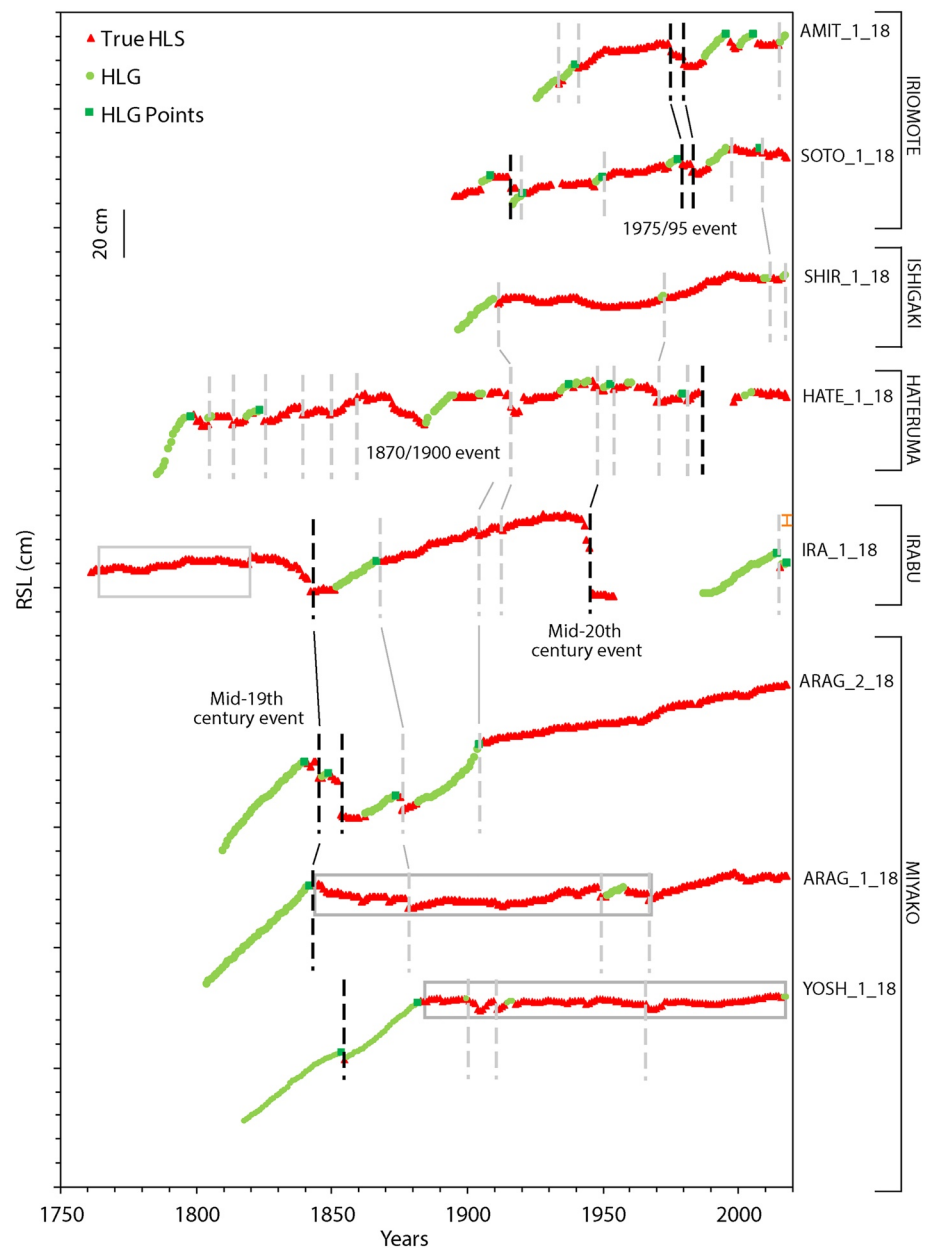


Figure 9. Relative sea level (RSL) variations of slices collected in the southern Ryukyu islands. Gray dashed lines indicate inferred climatic die-downs. Black dashed line show die-downs with uncertain origin, and associated with main RSL events identified in Figure 8. Light gray rectangles indicate periods of RSL variations with specific pattern (e.g., overturning in IRA_1_18, and possible moating in ARAG_1_18 and YOSH_1_18).

2001, and 2007. Those bleaching events may also induce changes in Porites microatolls growth rates (Rosenfeld et al., 2006; Suzuki et al., 2003). They are often due to an episode of increase of sea-surface temperature (SST) (Harii et al., 2014). Any of these episodes may correspond to the die-downs we observed (Figure 10), but at least two of them are associated with changes in the coral growth: the SST anomaly documented in 1983 (Harii et al., 2014) is synchronous with the death of colony A in HATE_1_18 slice in 1985 ± 2 . By contrast, the colony B of the same coral started to develop during the 1998 SST anomaly.

In Figure 11, we plotted the amplitude of the die-downs we observed in Yaeyama and Miyako areas. We observed that most of the die-downs have an amplitude below or equal to 5 cm, within their uncertainties range. Only three

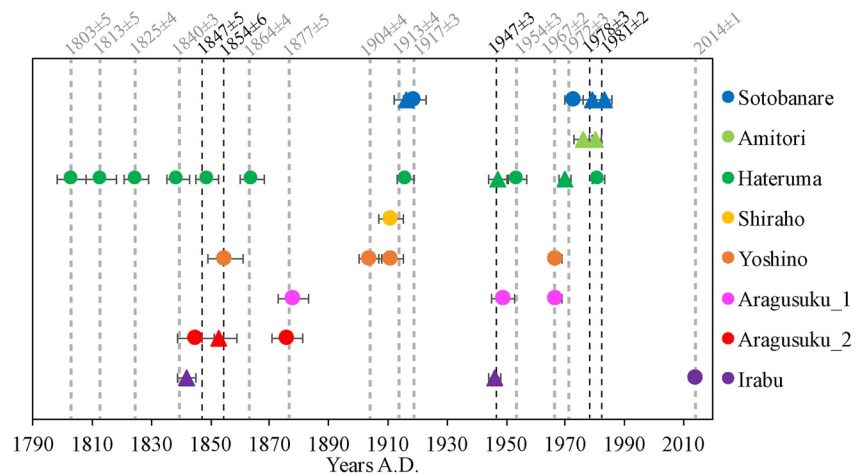


Figure 10. Summary of all die-downs recorded by the slices in the southern Ryukyus. Circles are for die-downs with supposed climatic origin, and triangles are for die-downs with uncertain origin. Die-downs resulting from comparison between all slices are indicated with dashed gray and black lines for climatic and undefined origin, respectively.

of them have significantly higher amplitude, larger than 10 cm. They occurred during the decadal RSL decreases of mid-19th century and mid-20th century, which were identified as events 1/2 and event 6 in IRA_1_18, respectively (Figure 8).

5.2. Climatic Source of the RSL Signal: Insight From Tide Gauge Data

To better understand the RSL changes and their sources, we analyzed the tidal records available around the southern Ryukyus (Figure 12). We selected five tide gauge stations from Permanent Service for Mean Sea-Level (PSMSL) data between Taiwan in the south and Naze on the Amami island in the north (locations in Figure 1; <https://www.psmsl.org/data/obtaining/>). The length of the record ranges between 38 years for Taiwan to 56 years for Naze.

All tidegraphs show mean relative submergence along the Ryukyu arc and in Taiwan. We calculated the long-term trend in RSL rate for each tide record by linear regression. The obtained value varies from 0.4 ± 0.1 to 3.0 ± 0.7 mm/yr in Taiwan and in Ishigaki, respectively. A first drop of 10 cm occurred in 1968 and was recorded by the Naze, Naha and Taiwan tide gauges. In 1979, a large drop of 7 cm in amplitude is observed by the Taiwan tidegraph and is also observable with a smaller amplitude at other sites. In 1984 the Ishigaki tide gauge documented a large drop of 7 cm in amplitude, which was also observed in Naha and Okinawa, and a few years later in Naze and Taiwan. We noted another main drop in 1993 in all tide gauge records, with an amplitude ranging

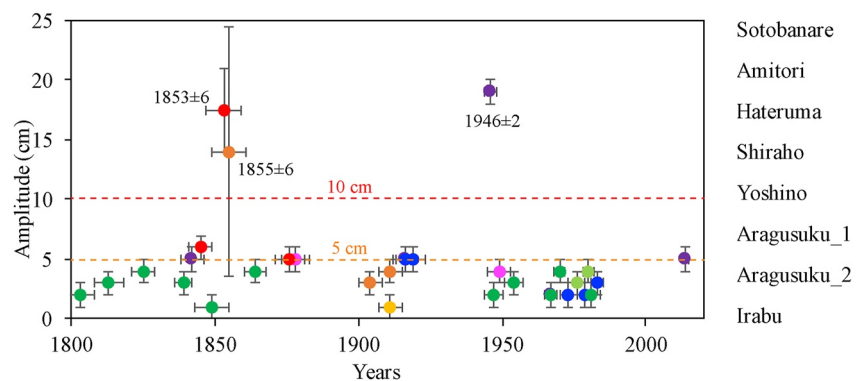


Figure 11. Amplitude of die-downs recorded by our slices. Uncertainties are of 1 cm on amplitude. Larger uncertainties are related to interpretation on minimum amplitude of die-downs in Yoshino and Aragusuku slices. Dashed orange and red lines are the selection threshold of 5 and 10 cm of amplitude, respectively.

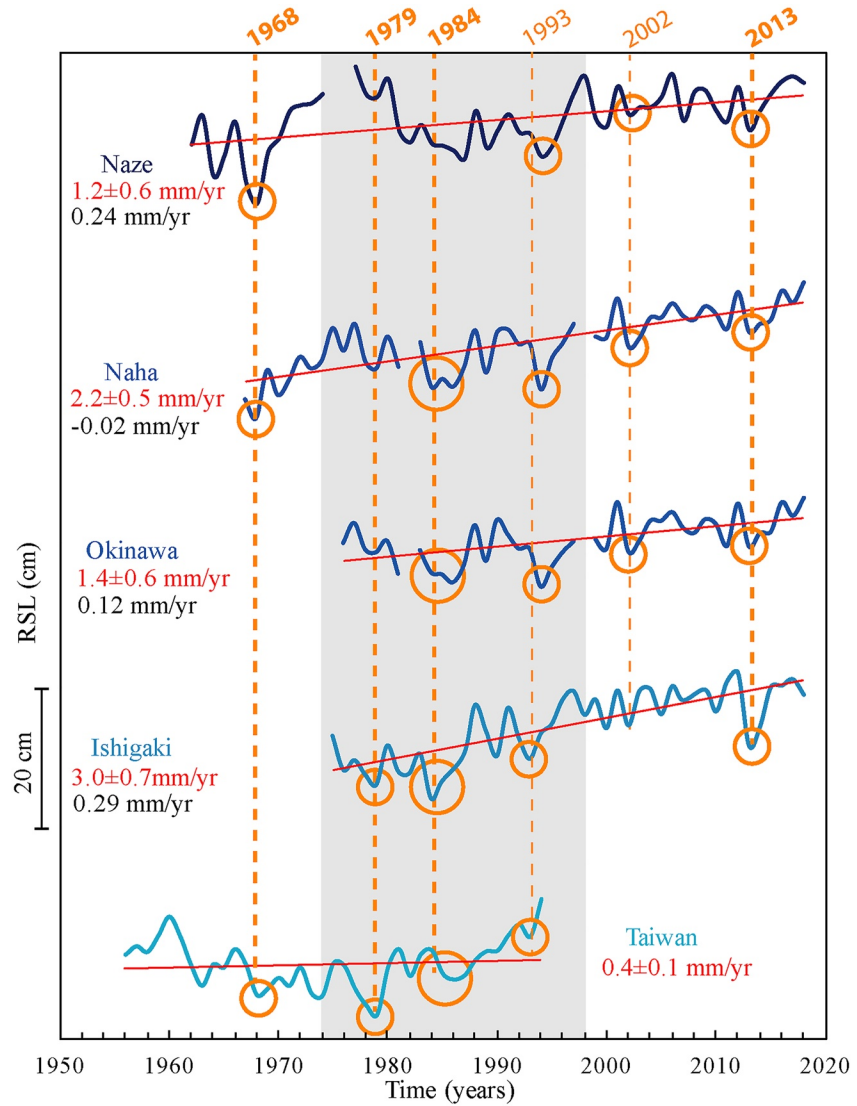


Figure 12. Tide gauges from Permanent Service for Mean Sea-Level tide gauge stations around the southern Ryukyus (location in Figure 1). Red lines are global trends estimated by linear regression. Black rates indicate tectonic uplift recorded by GPS between 1997 and 2017 (see Table 6). Orange circles and dashed lines are sea-level drops documented by our coral microatolls. Bold lines correspond to die-downs observed in the Highest Level of Survival curve of our microatolls. Gray area indicates the period of specific relative sea level pattern observed during events 8/9.

Table 6
Estimation of the Absolute Sea-Level Trend in the Ryukyu Archipelago Between 1997 and 2017

Location	GNSS station	Period	Tidegraph	GPS data	Absolute sea-level trend
Naze	950494	1 April 1996–31 January 2018	0.4	2.4	2.8
Naha	021096	1 May 2003–31 January 2018	1.2	−0.2	1.0
Okinawa	960745	1 April 1997–31 January 2018	1.2	1.2	2.4
Ishigaki	960750	1 April 1997–31 January 2018	0.8	2.9	3.7

Note. All rates are in mm/yr. Locations are indicated in Figure 1. Tide data are from PSMSL. GPS data are GNSS data obtained from Geospatial Information Authority of Japan (GSI). For the calculation of annual uplift (vertical velocity) by GNSS, we used the GNSS sites data of GEONET in the Ryukyu Islands which is operated by the GSI. We employed the vertical component of daily solutions of F3 (final) at the sites for the analysis. After removing the artificial height change due to the renewal of the equipment, the linear approximation was performed by the least squares method to obtain the secular change. In columns 4, 5, and 6, positive values indicate rising RSL, uplift and rising absolute sea-level, respectively. We do not use uncertainty as it is a first-order estimation.

between 2 and 7 cm. In 2002, a small drop of a few centimeters is observed mostly in the central Ryukyu stations. In 2013, the Ishigaki tide gauge recorded a large drop of 10 cm, which was also recorded by the Okinawa, Naha, and Naze tide stations.

As they are widely observed along the arc, those variations may be due to atmospheric and oceanic conditions that are dependent on the El Niño Southern Oscillation, which is a climatic mode occurring in the Pacific Ocean area and which can lead to inter-annual variations in the RSL records (Meysignac et al., 2012; Weil-Accardo et al., 2020). Those variations are observed in the RSL record of our microatolls.

Several die-down events identified from our HLS curves (Figure 10) are correlated with drops of the sea-level observed in tide gauge records (Figure 12), over the whole archipelago. In 1968 ± 2 , die-downs observed in HATE_1_18, ARAG_1_18, and YOSH_1_18 from Hateruma and Miyako islands could correspond to the 1968 drop, although their amplitude is smaller (less than 5 cm, Figures 10 and 11). The 1978 and 1984 drops in the tide gauge records could correspond to die-downs recorded in 1978 ± 3 and 1981 ± 2 in HATE_1_18, SOTO_1_18, and AMIT_1_18, as well as the 1975/1995 event observed in AMIT_1_18 and SOTO_1_18. However, we note that they were not observed in Miyako and Irabu islands. The 1993 and 2002 drops do not correspond to any die-downs in our slices record. Finally, only IRA_1_18 recorded a drop in 2014 ± 1 that could correspond to the 2013 drop in the tide gauge. As die-downs from the 1975/1995 were only observed in Iriomote and Hateruma islands, we propose that their origin is local and that drops of the sea-level only can not fully explain their occurrence.

5.2.1. Origin of Main Decadal Events

For periods older than 1960, we have no information from the tide-gauge record we used. It is thus difficult to discuss the origin of the decadal mid-19th, 1870–1900 and mid-20th century events.

None of these events was recorded by all microatolls so we can discard a regional or global climatic origin for those events.

Strong tropical storms and typhoons can promote sea-level rise or drop when they strike; for instance, a die-down of about 10 cm recorded in microatolls from Haiti was attributed to the passage of a large hurricane in 1963 (Weil-Accardo, Feuillet, Jacques, Deschamps, Beauducel, et al., 2016). Typhoon rainfalls can damage corals (Fabricius et al., 2008; Knowlton et al., 1981). They promote discharges of silt-sized and nutrient-rich sediments from rivers (Blanco et al., 2008; Harii et al., 2014; Ikeda et al., 2009), which can bury corals. The lowest part YOSH_1_18 was partly killed in 1947 over a thickness of 30 cm (Figure S1.5h in Supporting Information S1). This event is unlikely to be due to the compaction of the substrate as the coral quickly expanded downward in the following years, and the HLS elevation was almost unchanged before and after this event. The lowest part of YOSH_1_18 slice could have been covered by sediments during, for example, a storm.

Two strong tropical cyclones that hit the Japanese coasts were documented, one in 1853 mainly affecting the central Ryukyus, and one in 1863 extending from Miyako to the northern Ryukyus (Kubota et al., 2021). The 1863 typhoon could have impacted the microatolls but the sea-level drop would have been sudden (Weil-Accardo, Feuillet, Jacques, Deschamps, Saurel, et al., 2016; Figure 8) and it is not what we observed in any of the events 1 to 11 except event 6 in Irabu (19 cm in one year in 1946 ± 2). To our knowledge, no strong hurricane was reported in Irabu in this period. It is thus difficult to find other explanations on RSL changes than land motion.

For one of the most recent events—events 8 and 9, the tide gauge records are available. The pattern of those events 8 and 9 is recognized in the tide gauge records of Taiwan and Ishigaki, with a decrease of the RSL in two steps in 1979 and 1984, and a progressive RSL increase until 1997. The relative submergence during event 9 is a progressive rather than a sudden event. The RSL pattern of events 8 and 9 in the 1975–1995 period is mostly observed in the Ishigaki tidegraph whereas other tidegraphs only show a sea-level drop in 1984. In Naze, Naha and Okinawa, tidegraphs indicate a steady rather than an increasing RSL between 1984 and 1997. In the Taiwan tide record, RSL starts increasing at 1979 instead of 1984. Events 8 and 9 therefore likely result from a local rather than regional process, providing further support for a tectonic hypothesis.

Such decadal scale long-term RSL changes have been observed elsewhere and interpreted as long-lived SSEs (Mallick et al., 2021; Weil-Accardo et al., 2020). The duration of events is comparable to those described with microatolls studies in the Okinawa region (Weil-Accardo et al., 2020) and much longer than the longest SSEs detected by geodesy (few years, Obara & Kato, 2016). The longest event is 10 years longer than the long-lived

Table 7
Satellite Altimetry Trends From 1992 to 2020 From National Oceanic and Atmospheric Administration Data

Maritime area	Mean trend of satellite altimetry since 1992 (mm/yr)
Pacific Ocean	+2.7 ± 0.4
Northern Pacific Ocean	+2.9 ± 0.4
Yellow Sea	+2.5 ± 0.4

slow-slip event documented by Mallick et al. (2021). To our knowledge, it is the longest event ever documented. Their recurrence times vary between 10 and 40 years which is much larger than recurrence times of short-lived SSEs detected in other regions of Japan (Obara & Kato, 2016; Takagi et al., 2019) and in the Ryukyus (Heki & Kataoka, 2008) but comparable to other SSEs of the same magnitude documented by corals in the Okinawa region (Weil-Accardo et al., 2020).

5.2.2. Estimation of the Recent Absolute Sea-Level Changes

We attempted to estimate the climatic long-term component of the RSL signal documented by the microatolls. To that end, we correlated the RSL trend recorded by the tide gauge stations with the vertical crustal motion observed through GPS data. We use GPS vertical motions recorded by GPS stations (Figure 1 inset), collected over the period 1997–2017. We used tidegraphs from PSMSL (Figure 12), and we estimated the change of RSL rate at different tide stations of the archipelago over the 1997–2017 period. Data are summarized in Table 6. Over the 1997–2017 period, GPS data in Ishigaki indicate that the southern part of the island, including the tide gauge station, underwent an uplift of 2.9 mm/yr. Within this period, a relative sea-level rise was taking place at a rate of 0.8 mm/yr, which indicates a rough absolute sea-level increase of 3.7 mm/yr. We used the same approach for other stations where we have both tide and GPS data, and we obtained a first-order estimate of the absolute sea-level increase between 1.0 and 3.7 mm/yr in the archipelago, 2.5 ± 1.1 mm/yr on average.

We compared these measurements to satellite altimetry data from National Oceanic and Atmospheric Administration (Table 7). If our result is slightly lower than the mean trend of Pacific Ocean, which is a worldwide scale, or the trend for the northern Pacific Ocean, it corresponds to the mean trend for the Yellow Sea, which ends at the Okinawa Trough ($+2.5 \pm 0.4$ mm/yr). Furthermore, our result of 2.5 ± 1.1 mm/yr may be approximated by the absolute sea-level rise of 3 ± 1 mm/yr estimated by Meyssignac et al. (2012) and Meyssignac and Cazenave (2012) from sea-level reconstructions over 60 years in the Ryukyus.

In the southern Ryukyus, the significant variability of the RSL signal between our different samples differs from the homogeneous regional absolute sea-level rise of 2.5 ± 1.1 mm/yr. This variability is also observed in the tide gauge signals (Figure 12), which results from both tectonic and climate processes. These suggest an important tectonic component in the RSL is recorded in our microatolls.

By correcting the RSL signal from absolute sea-level estimated from GPS and tidegraph data, we retrieved the tectonic component of the RSL recorded in each microatoll. We estimate a regional sea-level increase rate of 2.5 ± 1.1 mm/yr for the 1997–2017 period, which is close to the value estimated by Meyssignac and Cazenave (2012) since 1950, for example, 3 ± 1 mm/yr. As this last value is defined over a larger time period, we use it to correct the mean RSL rates of the living period of the microatolls. The relative vertical motion recorded by the microatolls during their lives corresponds to uplift ranging between 0.7 ± 1.5 and 2.8 ± 1.5 mm/yr (Table 4, last column).

5.3. Source of the Tectonic RSL Changes

As a significant tectonic component was identified in our microatolls, we discuss in the following the origin of this vertical deformation.

5.3.1. Local Tectonic

In the southern Ryukyus, no subaerial volcano has been documented and the volcanic front is ambiguous. It is inferred to be located less than 40 km north of Miyako island (Minami & Ohara, 2018). At this distance, volcanic activity is too far (more than 300 km) from the southern islands to induce deformation recorded by our microatolls, and the same holds for active volcanoes identified within the Okinawa Trough in front of the central island arc. Moreover, a submarine eruption was reported in 1924 off Iriomote island, but with no clear evidence for its precise origin (Kato, 1982). No event of that age was found in the closest sliced corals, which are SOTO_1_18, AMIT_1_18, and SHIR_1_18, and no sign of volcanic activity has been reported ever since.

The sites we studied are located south of the active Okinawa rift, where several normal faults accommodate a total spreading rate of 50 mm/yr (Y.-J. Hsu et al., 2012; Sibuet et al., 1987). This would imply slip rate of few mm/yr

along individual normal faults. The site of Sotobanare is the closest from the rift and is located 15 km far from the main southern bounding fault (Figure 3).

Onshore, the islands of Irabu and Miyako are affected by another family of NNW-SSE trending local faults, i.e. faults perpendicular to the arc. They result from an extensional stress field parallel to the trench (Fournier et al., 2001; Kubo & Fukuyama, 2003; Otsubo & Hayashi, 2003). The main faults of this family crosscut the arc offshore (Miyako Saddle, Kerama gap (Figures 1 and 3) (Matsumoto et al., 2009; Nakamura, 2006; Figure 3), and are located up to 30 km away from our site of study. Slip rates on similar faults were inferred to be 0.1 mm/yr by K. Arai et al. (2018) in Okinawa area.

As observed and modeled elsewhere, surface deformations due to motion on the crustal faults of the Okinawa rift or on the second arc-perpendicular family, would be limited within a radius equal to the fault depth (at most tens of kilometers as the seismogenic upper crust is about 15 km, King et al., 1988). Those faults are thus likely too far or too slow to account for the variations of the RSL we document. We checked however with simple elastic models presented below that slip on the main southern normal fault bounding the Okinawa trough promotes negligible vertical deformations at our sampling sites.

We thus consider that most of the RSL signal recorded by the coral microatolls in this study is related to processes at the subduction plate interface.

5.3.2. Megathrust Seismic Cycle

The main steady uplift recorded by the microatolls (Table 4) throughout their life may correspond to interseismic loading along the plate interface. In the Miyako area, which is located 45 km from the trench, living microatolls have recorded uplift with rates ranging between 0.7 ± 1.5 and 2.1 ± 1.1 mm/yr in the Aragusuku and Yoshino sites, respectively, and uplift of 2.8 ± 1.5 mm/yr in Irabu island. In the Yaeyama islands (i.e., between Yonaguni and Ishigaki islands, see Figure 1), living microatolls have recorded uplift with rates ranging between 1.3 ± 1.1 and 1.9 ± 1.2 mm/yr in Ishigaki and Iriomote islands, at distances ranging between 134 and 129 km from the trench, respectively. In Hateruma, which is the closest island from the trench (97 km), we document a steady uplift of 2.5 ± 1.1 mm/yr. At smaller time scale, we observe change in interseismic rates through time. Such changes have been documented elsewhere (Meltzner et al., 2015; Weil-Accardo et al., 2020) and could indicate a change of the interplate seismic coupling or of the location of the coupled area.

Decadal scale events 1–11 have also been observed in the RSL records.

In terms of amplitude, the main events, which occurred in the mid-19th century, that is, between 1870 and 1900, and between 1975 and 1995, may be transient events related to aseismic slips on the megathrust. For events 8/9 in 1975/1995, this hypothesis is also supported by the observation of a subsidence of up to 4 cm observed in western Iriomote island following earthquake swarms between 1991 and 1992 (Report of the coordinating Committee for Earthquake Prediction, Japan, 1993).

To better constrain the seismic coupling and the origin of the possible transient deformations observed in the coral records, we used simple 2D elastic dislocation models (Kanda & Simons, 2010, 2012; Okada, 1992; Savage, 1983). The strategy is fully described in Weil-Accardo et al. (2020).

We also modeled short-term vertical deformations that we deduced from GNSS records (Table 8). We used records of short-term vertical motions that are provided by the Geospatial Information Authority of Japan (GSI) between 1997 and 2018. We documented an uplift in the past 20 years that varies between 0.0 and 1.6 mm/yr in the Miyako island area, and between 0.6 and 6.5 mm/yr in the Yaeyama islands.

5.4. Elastic Modeling

We used the megathrust geometry derived from SLAB 2.0 (Hayes et al., 2018) that compiles all available data from geophysical investigation. We checked the consistency of the SLAB2.0 models with seismic results around Ishigaki and Miyako islands (R. Arai et al., 2016; S.-K. Hsu et al., 2013; Nishizawa et al., 2017). We chose to model the plate interface with two faults for simplicity (see details below).

The results are presented in Figures 13 and 14.

Table 8

Short-Term Vertical Motions Recorded by GPS Stations in the Southern Ryukyus Between 1997 and 2017

Latitude	Longitude	Islands	GNSS station	Period	Distance to trench (km)	Uplift (mm/yr)
125.3738	24.75312	Miyako	950498	1 April 1996–31 January 2018	148	0.7
125.17098	24.82795	Irabu	960747	1 April 1997–31 January 2018	166	0.0
124.69244	24.64161	Tarama	960748	1 April 1997–31 January 2018	164	1.6
122.94285	24.45416	Yonaguni	950499	1 April 1996–5 December 2013	147	6.5
123.79204	24.42627	Iriomote	950500	1 April 1996–31 January 2018	139	0.6
124.30129	24.53662	Ishigaki	960749	1 April 1997–31 January 2018	148	2.2
124.17265	24.33887	Ishigaki	960750	1 April 1997–31 January 2018	127	2.9
123.79585	24.06149	Hateruma	960751	1 April 1997–31 January 2018	97	1.9

Note. For the calculation of annual uplift (vertical velocity) by GNSS, we used the GNSS sites data of GEONET in the Ryukyu Islands which is operated by the Geospatial Information Authority of Japan (GSI). We employed the vertical component of the daily solution of F3 (final) at the sites for the analysis. After removing the artificial height change due to the renewal of the equipment, the linear approximation was performed with the least squares method to obtain the secular change.

5.4.1. Interseismic Deformation

To model the long-term vertical deformation, we used the classical back-slip models on the shallow plate interface (fault 1, red lines on Figure 13) of Savage (1983). Data are from our microatolls records in sites and the GNSS data, that are located 97–166 km away from the trench (purple points in Figure 13). For a curved slab

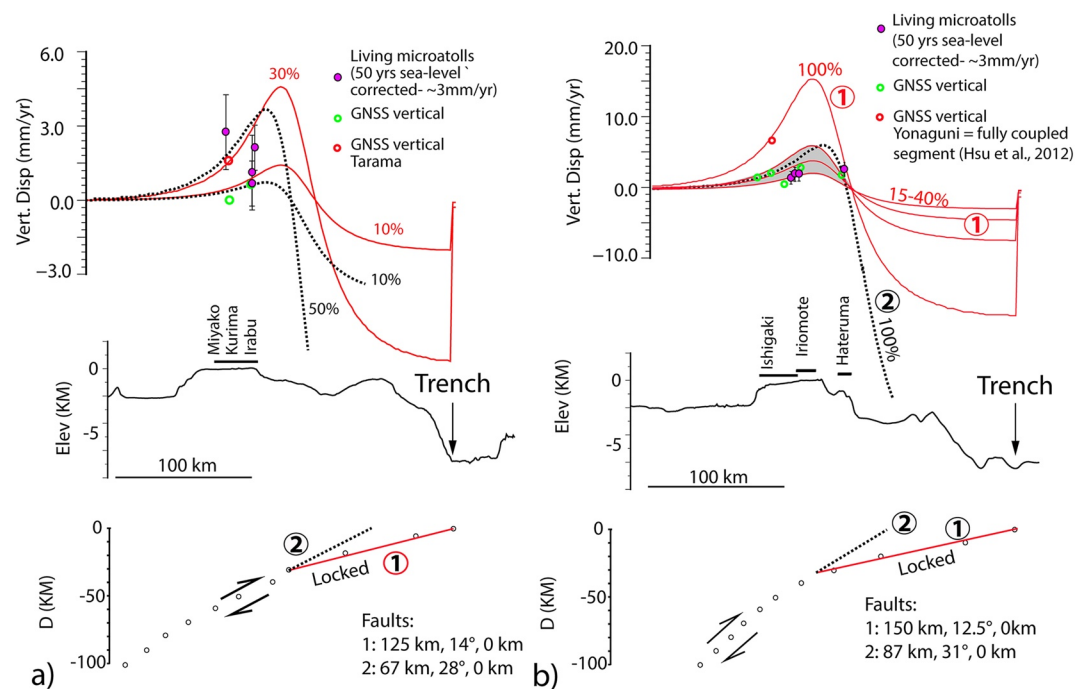


Figure 13. 2D Elastic models of the interseismic deformation in (a) Miyako area and (b) Ishigaki area. All models are performed in an elastic half space with $\lambda = \mu = 32$ GPa. Slab depth is from the SLAB2.0 model (Hayes et al., 2018), topography from SRTM15+ (Tozer et al., 2019). Green dots: value of the Global Navigation Satellite Systems (GNSS) GPS vertical motion in southern Ryukyus (Table 8). Red dots: value of the GNSS GPS vertical motion in (a) Tarama and (b) Yonaguni islands (Table 8). Purple dots are interseismic uplift values estimated from recent microatolls in southern Ryukyu islands corrected with a sea-level rise of ~ 3 mm/yr (Meyssignac et al., 2012). Red curve: vertical deformation rate promoted by backslip along the dislocation (fault 1). Dashed black curve: vertical deformation rate (mm/yr) promoted by backslip along fault 2 between 0 and 60 km using theoretical faults tangential to megathrust kink (Kanda & Simons, 2012). (b) Dark gray area: vertical deformation rate promoted by backslip with seismic coupling between 15% and 40% along fault 1 between 0 and 35 km.

geometry, Kanda and Simons (2012) showed that, at a distance beyond two times the depth of locking, the surface deformation can be approximated by locking along a planar fault tangential to the curved interface near the bottom of the locked zones. As the slab is curved, we thus also tested the back-slip models on a steeper fault (fault 2, dashed lines on Figures 13a and 13b). We varied the coupling rate between 0% and 100% (back-slip ranging between 0 and 8 cm/yr). Fault parameters are indicated in the bottom part of Figures 13a and 13b).

We also modeled the short-term vertical deformation recorded by GPS between 1997 and 2017 in the Miyako area (Miyako, Irabu, and Tarama Islands) ranging between 0.0 and 1.6 mm/yr (see all values in Table 8, green and red points).

In both Miyako (Figure 13a) and Ishigaki (Figure 13b), we modeled the vertical deformations recorded by microatolls and GNSS data by coupling on both fault models. By using the more realistic model for a curved slab (fault 2) instead of the classical one (fault 1), the coupling rate must be larger to model the deformation: between 10% and 50% in Miyako and 100% in Ishigaki versus 10%–30% for Miyako and 15%–40% for Ishigaki, and even 100% for Yonaguni in agreement with Y.-J. Hsu et al. (2012). Those values are comparable or higher than those previously estimated from GNSS data and confirm that the megathrust is loading. The coupling depth deduced from our models is about 40 km, comparable to that observed in other subduction zones (i.e., Chlieh et al., 2007). It is noteworthy that this depth corresponds to the updip limit of the zone where SSEs occurred in Ishigaki (Nishimura, 2014, Figure 2b). This is classically observed in other regions of Japan (Obara & Kato, 2016).

5.4.2. Transient Events

We model the decadal-scale transient sea-level changes (by considering that they are all transient aseismic events as discussed previously [Events 1–11, Figure 8 and values in Table 5]). We plotted the land-level change rates in cm/yr deduced from the amplitude and duration of each event and corrected from the global sea-level change (value presented in Table 5, column 6). We tested dislocations on different portions of the megathrust interface: above 40 km depth (fault 1), below 40 km (fault 2, with a downdip limit of the fault as deep as 80 km), and both faults (1 + 2). The faults parameters are indicated in the bottom part of Figure 14.

Both in Miyako and Yaeyama islands, long-lived events of subsidence can be modeled by slow slips in the shallow portion of the megathrust (in the seismogenic coupled zone, fault 1). By contrast, the long-lived events of uplift can be modeled by slip in the deeper portion of the megathrust below the coupling zone (between 40 and 80 km) or by slip on the entire portion of the megathrust (Fault 1 + 2). The depth range of those deep SSEs is comparable to that of SSEs identified in northern Japan (between 30 and 70 km, Khoshmanesh et al., 2020). Except for Event 6 in Irabu (purple star on Figure 14) which is much larger than the others, the slow-slip event rates deduced from our modeling range between 3 and 9 cm/yr. This is to 0.3–1.1 times the long-term subduction rate, slightly lower than that observed for the 32 years long slow-slip event in Sumatra (Mallick et al., 2021). During an event, the total slips released by the SSEs on the megathrust range between 24 and 210 cm, compatible with SSEs identified in western Nankai (Japan, Takagi et al., 2019).

The uplift event of 19 cm recorded in one year in Irabu (purple star) may have been promoted by a slip ranging between 60 and 95 cm/yr depending on the fault model we used (Figure 14). In total the SSEs released 7 m of slip along the megathrust between ~1850 and today. This is about 50% of the total convergence, a value similar to that estimated in western Nankai (Takagi et al., 2019). As our models are 2D models, we cannot estimate a magnitude. By considering slip of 24–210 cm on a 100-long and 80 km-wide zone corresponding to the dimension of the area where the SSEs occur beneath Yaeyama islands (Nishimura, 2014), the magnitude of the SSEs recorded by the coral would range between 7 and 7.7. This magnitude is comparable to that of major SSEs recorded in subduction zones worldwide (Mallick et al., 2021; Obara & Kato, 2016; Takagi et al., 2019) and larger than the largest SSE observed by geodetic data in the Yaeyama islands (M6.5, Nishimura, 2014).

We showed that the SSEs occurred in pair. To our knowledge, this was never documented before.

This could suggest that the SSEs would occur first below the coupling zone (e.g., at depth ranging between 40 and 80 km) before migrating along the shallower coupled part of the megathrust (e.g., above 40 km, Nakamura, 2017). The SSEs may have promoted stress changes leading to an increase in the seismic activity as observed in New-Zealand (Bartlow et al., 2014). SSEs can also precede large subduction earthquakes as observed for example, before the 2011 Tohoku earthquake in Japan (Obara & Kato, 2016), or before the 2014 Iquique earthquake in Chile (Ruiz et al., 2014). Slow-slip events can contribute to unlocking the plate interface and trigger

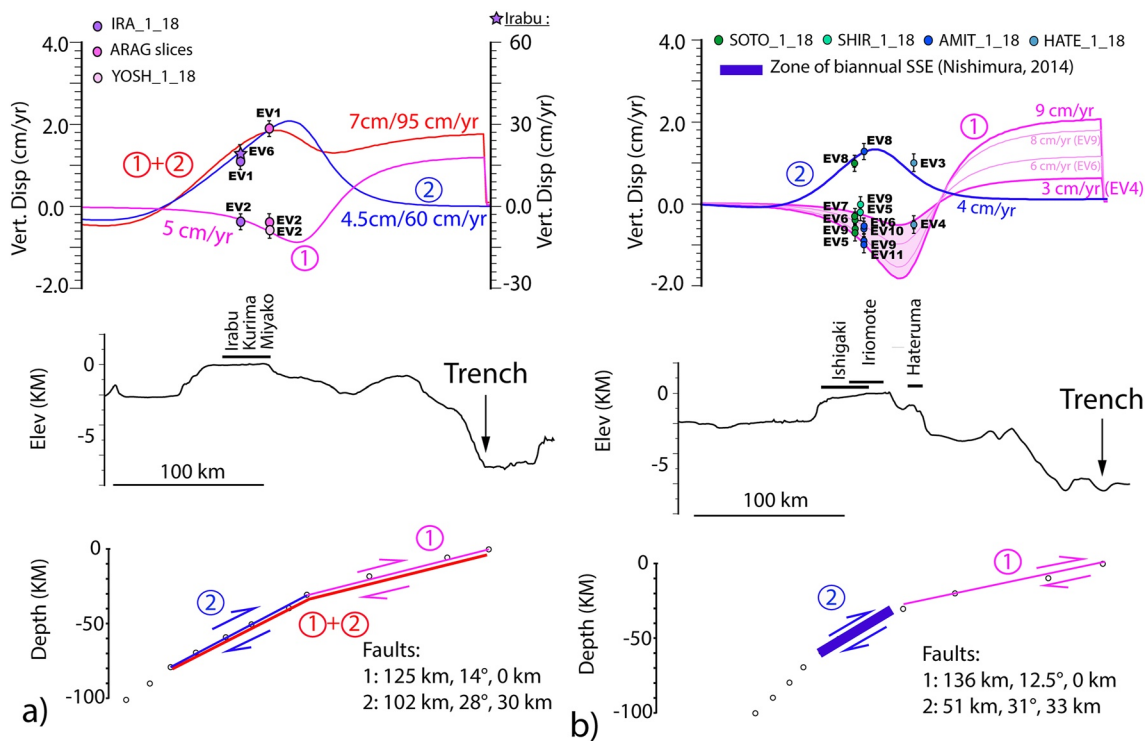


Figure 14. 2D Elastic models of the aseismic deformations in (a) Miyako area and (b) Ishigaki area. All models are performed in an elastic half space $\lambda = \mu = 32$ GPa. Slab depth as in Figure 13. (a) Aseismic motion recorded during events 1, 2, and 6 in IRA_1_18, ARAG_2_18, and YOSH_1_18 slices. Pink curve: vertical deformation at the surface promoted by slips of 5 cm/yr on fault 1 between 0 and 30-km depth. Blue curve: vertical deformation at the surface promoted by slips of 4.5 cm/yr on the fault 2 between 30 and 80-km depth. This curve also shows slip of 60 cm/yr in the same area for event 6 in Irabu site (right axis). Red curve: vertical deformation at the surface promoted by slips of 7 and 95 cm/yr on fault 1 + 2 between 0 and 80-km depth, to reproduce event 1 and 6 motions, respectively. (b) Aseismic motion recorded during events 3–11 in AMIT_1_18, SOTO_1_18, SHIR_1_18, and HATE_1_18 slices. Blue curve: vertical deformation at the surface promoted by slip of 4 cm/yr on fault 2 between 30 and 60-km depth. Pink area: vertical deformation at the surface promoted by slips between 3 and 9 cm/yr on fault 1 between 0 and 30-km depth.

large earthquake or/and an increase of seismicity (Obara & Kato, 2016). Their presence has an important implication for the seismic hazard in this area.

As our data set is limited to a few sites, we used a simple elastic dislocation model to model the vertical deformations induced by SSEs at the plate interface. More complex models involving plastic creep in the fore-arc (power law rheologies, applied to afterslip) concluded that the depth of afterslip could be overestimated by simple linear elastic models (Peña et al., 2020). We cannot exclude that simple elastic models used in this study overestimated the depth of the SSEs.

6. Conclusion

We reconstructed the relative sea-level changes over the last two centuries using modern coral microatolls in the southern Ryukyus. We aimed to gain information on the seismic cycle of the subduction zone on a poorly known region. We sampled eight microatolls slabs in seven sites, located in fringing reefs surrounding the islands of Miyako, Irabu, Hateruma, Ishigaki, and Iriomote. We prepared the slabs to image them with X-Ray and CT-scan. Combination of those images revealed the growth bands in great details, and we established the chronology of the RSL by counting those growth bands. For slabs with complex morphologies or fossil dead parts, the band counting was calibrated by 7 U/Th dating.

Microatolls recorded RSL changes with various durations and amplitudes that are either of tectonic or climatic origin. All microatolls recorded a long-lived mean relative submergence at rates ranging between 0.2 ± 0.5 and 2.3 ± 0.5 mm/yr. In addition to this long-term trend, they all recorded multi-decadal RSL changes with 2–29 cm in amplitude. The recurrence time of those events varies between 10 and 40 years. Finally, as observed elsewhere,

the microatolls recorded climatic temporary die-downs of a few centimeters subsidence at a regional scale, that is, on both Miyako and Yaeyama islands. We used tide gauge data to discuss the source of the different events we identified, and decipher the tectonic component of the RSL change. Using satellite altimetry, and tidegraphs combined with vertical GPS motion, we estimated that the absolute sea-level change is about 3 ± 1 mm/yr. We corrected the microatolls RSL signal from this value to estimate the magnitude of the land motion. We discussed the origin of the land motion and inferred that it is related to the seismic cycle of the megathrust.

We modeled the vertical land motion recorded by the microatolls by simple dislocation models in an elastic half-space. We simulated the strain accumulation during the interseismic period (in between earthquakes) by classical back-slip models. Depending on the models, we estimated coupling rates between 10% and 50% in Miyako and between 15% and 100% in the Yaeyama islands. This is higher than the coupling rate estimated from GNSS data (35%). The models showed that the downdip limit of the coupling zone is around 40 km deep. Our results confirm that a significant part of the plate convergence is accumulating along a locked plate interface. The last dramatic event occurred in 1771 in the area (Meiwa tsunami). The origin of the tsunami is still debated but considering that this earthquake ruptured the plate interface, 0.8–8 cm/yr of slip deficit would have accumulated over the last 250 years. This corresponds to a total slip deficit ranging between 2 and 20 m, depending on the coupling rate. This may be sufficient to promote a large earthquake in the area in a near future.

Multidecadal (duration between 1 and 42 years) RSL changes are likely surface deformations due to SSEs at a rate of 3–9 cm/yr (with an extreme value of 60 or 95 cm/yr). Elastic models indicated that the slow-slip occurred either in the deeper part of the plate interface, below the coupling zone, or above. The recurrence time of those events varies between 10 and 40 years and in total they accommodated about 50% of the total convergence since the mid-19th century. This percentage is similar to that observed in other parts of the subduction zone in Japan. We estimated an event magnitude ranging between 7 and 7.7 for those SSEs, comparable to that of the major SSEs observed worldwide with geodetic data. The events occurred in pairs (relative sea-level drops followed by relative sea-level rises of the same amplitude) suggesting that the SSEs nucleated in the deeper portion and migrated upwards. Upward migration of SSEs was observed before the 2014 Iquique earthquake in Chile (Ruiz et al., 2014). In Yaeyama islands, the deep SSEs we documented are located in the same area as biannual smaller SSEs documented by geodetic data. Both short and long-lived SSEs may contribute to transfer of stress to the megathrust and triggering of its rupture during a large subduction earthquake. Our results provide new important constraints of seismic hazard in the Ryukyu subduction zone.

Data Availability Statement

Analyzed data (X-ray and scan images of the corals, HLS curves) are available on the following link: <https://figshare.com/s/741d02561fbb263b9b96>. We used the GMT software developed by P. Wessel and W. Schmith available at <https://www.generic-mapping-tools.org> for Figures 1 and 3.

References

- Ando, M., Kitamura, A., Tu, Y., Ohashi, Y., Imai, T., Nakamura, M., et al. (2018). Source of high tsunamis along the southernmost Ryukyu trench inferred from tsunami stratigraphy. *Tectonophysics*, 722, 265–276. <https://doi.org/10.1016/j.tecto.2017.11.007>
- Ando, M., Nakamura, M., Matsumoto, T., Furukawa, M., Tadokoro, K., & Furumoto, M. (2009). Is the Ryukyu subduction zone in Japan coupled or decoupled? —The necessity of seafloor crustal deformation observation. *Earth Planets and Space*, 61(9), 1031–1039.
- Ando, M., Tu, Y., Kumagai, H., Yamanaka, Y., & Lin, C.-H. (2012). Very low frequency earthquakes along the Ryukyu subduction zone. *Geophysical Research Letters*, 39(4), L04303.
- Arai, K., Inoue, T., & Sato, T. (2018). High-density surveys conducted to reveal active deformations of the upper forearc slope along the Ryukyu Trench, western Pacific, Japan. *Progress in Earth and Planetary Science*, 5(1), 1–15.
- Arai, R., Takahashi, T., Kodaira, S., Kaiho, Y., Nakanishi, A., Fujie, G., et al. (2016). Structure of the tsunamigenic plate boundary and low-frequency earthquakes in the southern Ryukyu Trench. *Nature Communications*, 7(1), 12255.
- Araoka, D., Yokoyama, Y., Suzuki, A., Goto, K., Miyagi, K., Miyazawa, K., et al. (2013). Tsunami recurrence revealed by Porites coral boulders in the southern Ryukyu Islands, Japan. *Geology*, 41(8), 919–922.
- Bartlow, N. M., Wallace, L. M., Beavan, R. J., Bannister, S., & Segall, P. (2014). Time-dependent modeling of slow slip events and associated seismicity and tremor at the Hikurangi subduction zone, New Zealand. *Journal of Geophysical Research: Solid Earth*, 119(1), 734–753.
- Blanco, A. C., Nadaoka, K., & Yamamoto, T. (2008). Planktonic and benthic microalgal community composition as indicators of terrestrial influence on a fringing reef in Ishigaki Island, Southwest Japan. *Marine Environmental Research*, 66(5), 520–535.
- Briggs, R. W., Sieh, K., Meltzner, A. J., Natawidjaja, D., Galetzka, J., Suwargadi, B., et al. (2006). Deformation and slip along the Sunda megathrust in the great 2005 Nias-Simeulue earthquake. *Science*, 311(5769), 1897–1901.
- Chappell, J., Chivas, A., Wallensky, E., Polach, H. A., & Aharon, P. (1983). Holocene palaeo-environmental changes, central to north Great Barrier Reef inner zone. *BMR Journal of Australian Geology and Geophysics Canberra*, 8, 223–235.

Acknowledgments

The authors are grateful to all the people who helped in the sampling and the analysis of the coral slices. A special thanks to H. Carton for the fruitful proofreading and advices on the manuscript. The corals were sliced thank to the Milano Industry Co. Ltd (Ogyu Manufacturing Inc.). The slices were X-rayed with the kind help of Prof. M. Mochizuki from the Department of Veterinary Medical Sciences, the University of Tokyo, and CT-scanned with the contribution of K. Seike's team from National Institute of Advanced Industrial Science and Technology (AIST). We are also very grateful to J. Weil-Accardo for her helpful advices on the coral analysis process. We are grateful to the reviewers O. Oncken and J. Zachariassen for constructive remarks that helped improve the manuscript. Field work and coral analyses were funded by the JSPS KAKENHI Grant JP16H01838. U/Th dating was supported by Grants from the Science Vanguard Research Program of the Ministry of Science and Technology, Taiwan, ROC (110-2123-M-002-009), the Higher Education Sprout Project of the Ministry of Education, Taiwan, ROC (110L901001 and 110L8907), and the National Taiwan University (109L8926) to C.-C.S. This work was supported by the Institut National des Sciences de l'Univers, Centre National de la Recherche Scientifique (CNRS-INSU Alea program 2019), the Institut de Physique du Globe de Paris (BQR IPGP 2018), the Ministère de l'enseignement supérieur, de la Recherche et de l'Innovation and the Ecole Doctorale UPC-IPGP. This is IPGP contribution 4277.

- Cheng, H., Edwards, R. L., Hoff, J., Gallup, C. D., Richards, D. A., & Asmerom, Y. (2000). The half-lives of uranium-234 and thorium-230. *Chemical Geology*, 169(1), 17–33.
- Cheng, H., Lawrence Edwards, R., Shen, C.-C., Polyak, V. J., Asmerom, Y., Woodhead, J., et al. (2013). Improvements in ²³⁰Th dating, ²³⁰Th and ²³⁴U half-life values, and U–Th isotopic measurements by multi-collector inductively coupled plasma mass spectrometry. *Earth and Planetary Science Letters*, 371–372, 82–91.
- Chlieh, M., Avouac, J. P., Hjorleifsdottir, V., Song, T. R. A., Ji, C., Sieh, K., et al. (2007). Coseismic slip and afterslip of the great M_w 9.15 Sumatra–Andaman earthquake of 2004. *Bulletin of the Seismological Society of America*, 97(1A), S152–S173.
- Cloos, M. (1992). Thrust-type subduction-zone earthquakes and seamount asperities: A physical model for seismic rupture. *Geology*, 20(7), 601–604.
- Denis, V., Mezaki, T., Tanaka, K., Kuo, C. Y., De Palmas, S., Keshavmurthy, S., & Chen, C. A. (2013). Coverage, diversity, and functionality of a high-latitude coral community (Tatsukushi, Shikoku Island, Japan). *PLoS One*, 8(1), e54330.
- Dominguez, S., Lallemand, S. E., Malavieille, J., & von Huene, R. (1998). Upper plate deformation associated with seamount subduction. *Tectonophysics*, 293(3), 207–224.
- Doo, W. B., Lo, C. L., Wu, W. N., Lin, J. Y., Hsu, S. K., Huang, Y. S., & Wang, H. F. (2018). Strength of plate coupling in the southern Ryukyu subduction zone. *Tectonophysics*, 723, 223–228.
- Fabricius, K. E., De'Ath, G., Puotinen, M. L., Done, T., Cooper, T. F., & Burgess, S. C. (2008). Disturbance gradients on inshore and offshore coral reefs caused by a severe tropical cyclone. *Limnology and Oceanography*, 53(2), 690–704.
- Fournier, M., Fabbri, O., Angelier, J., & Cadet, J. P. (2001). Regional seismicity and on-land deformation in the Ryukyu arc: Implications for the kinematics of opening of the Okinawa Trough. *Journal of Geophysical Research*, 106(B7), 13751–13768.
- Goto, H., Arai, K., & Sato, T. (2018). Topographic Anaglyphs from detailed digital elevation models covering inland and seafloor for the tectonic geomorphology studies in and around Yoron Island, Ryukyu arc, Japan. *Geosciences*, 8(10), 363.
- Goto, K., Kawana, T., & Imamura, F. (2010). Historical and geological evidence of boulders deposited by tsunamis, southern Ryukyu Islands, Japan. *Earth-Science Reviews*, 102(1), 77–99.
- Goto, K., Miyagi, K., & Imamura, F. (2013). Localized tsunamigenic earthquakes inferred from preferential distribution of coastal boulders on the Ryukyu Islands, Japan. *Geology*, 41(11), 1139–1142.
- Goto, K., Miyagi, K., Kawamata, H., & Imamura, F. (2010). Discrimination of boulders deposited by tsunamis and storm waves at Ishigaki Island, Japan. *Marine Geology*, 269(1), 34–45.
- Harii, S., Hongo, C., Ishihara, M., Ide, Y., & Kayanne, H. (2014). Impacts of multiple disturbances on coral communities at Ishigaki Island, Okinawa, Japan, during a 15-year survey. *Marine Ecology Progress Series*, 509, 171–180.
- Hayes, G. P., Moore, G. L., Portner, D. E., Hearne, M., Flamme, H., Furtney, M., & Smoczyk, G. M. (2018). Slab2, a comprehensive subduction zone geometry model. *Science*, 362(6410), 58–61.
- Heki, K., & Kataoka, T. (2008). On the biannually repeating slow-slip events at the Ryukyu Trench, southwestern Japan. *Journal of Geophysical Research*, 113(B11), B11402.
- Hiess, J., Condon, D. J., McLean, N., & Noble, S. R. (2012). ²³⁸U/²³⁵U systematics in terrestrial uranium-bearing minerals. *Science*, 335(6076), 1610–1614.
- Hongo, C., & Kayanne, H. (2009). Holocene coral reef development under windward and leeward locations at Ishigaki Island, Ryukyu Islands, Japan. *Sedimentary Geology*, 214(1), 62–73.
- Hopley, D. (1986). Corals and reefs as indicators of paleo-sea levels with special reference to the Great Barrier Reef. In O. V. van de Plasche (Ed.), & GeoBooks (Eds.), *Sea-Level research: A manual for the collection and evaluation of data*.
- Hsu, S.-K., & Sibuet, J.-C. (2005). Earthquake off Japan could generate strong tsunami arrays. *Eos, Transactions American Geophysical Union*, 86(17), 169–170.
- Hsu, S.-K., Yeh, Y.-C., Sibuet, J.-C., Doo, W.-B., & Tsai, C.-H. (2013). A mega-splay fault system and tsunami hazard in the southern Ryukyu subduction zone. *Earth and Planetary Science Letters*, 362, 99–107.
- Hsu, Y.-J., Ando, M., Yu, S.-B., & Simons, M. (2012). The potential for a great earthquake along the southernmost Ryukyu subduction zone. *Geophysical Research Letters*, 39(14), L14302.
- Ikedo, S., Osawa, K., & Akamatsu, Y. (2009). Sediment and nutrients transport in watershed and their impact on coastal environment. *Proceedings of the Japan Academy, Series B*, 85(9), 374–390.
- Jaffey, A., Flynn, K., Glendenin, L., Bentley, W. t., & Essling, A. (1971). Precision measurement of half-lives and specific activities of U 235 and U 238. *Physical Review C*, 4(5), 1889–1906.
- Kan, H. (2011). Ryukyu islands. *Encyclopedia of Earth Sciences Series, Part 2*, 940–945.
- Kanda, R. V. S., & Simons, M. (2010). An elastic plate model for interseismic deformation in subduction zones. *Journal of Geophysical Research*, 115(B3), B03405.
- Kanda, R. V. S., & Simons, M. (2012). Practical implications of the geometrical sensitivity of elastic dislocation models for field geologic surveys. *Tectonophysics*, 560–561, 94–104.
- Kao, H., Shen, S. J., & Ma, K.-F. (1998). Transition from oblique subduction to collision: Earthquakes in the southernmost Ryukyu arc-Taiwan region. *Journal of Geophysical Research*, 103(B4), 7211–7229.
- Kato, Y. (1982). Position and amount of erupted pumice from the Iriomote submarine volcano, Ryukyu Islands. *Ryukyu Isl*, 6, 41–47.
- Khoshramesh, M., Shirzaei, M., & Uchida, N. (2020). Deep slow-slip events promote seismicity in northeastern Japan megathrust. *Earth and Planetary Science Letters*, 540, 116261.
- King, G. C. P., Stein, R. S., & Rundle, J. B. (1988). The growth of geological structures by repeated earthquakes 1. Conceptual framework. *Journal of Geophysical Research*, 93(B11), 13307–13318.
- Knowlton, N., Lang, J. C., Christine Rooney, M., & Clifford, P. (1981). Evidence for delayed mortality in hurricane-damaged Jamaican staghorn corals. *Nature*, 294(5838), 251–252.
- Konishi, K., & Sudo, K. (1972). From the Ryukyus to Taiwan. *Kagaku (Science)*, 42, 271–280.
- Kubo, A., & Fukuyama, E. (2003). Stress field along the Ryukyu Arc and the Okinawa Trough inferred from moment tensors of shallow earthquakes. *Earth and Planetary Science Letters*, 210(1–2), 305–316.
- Kubota, H., Matsumoto, J., Zaiki, M., Tsukahara, T., Mikami, T., Allan, R., et al. (2021). Tropical cyclones over the western north Pacific since the mid-nineteenth century. *Climatic Change*, 164(3), 29.
- Leclerc, F., & Feuillet, N. (2019). Quaternary coral reef complexes as powerful markers of long-term subsidence related to deep processes at subduction zones: Insights from Les Saintes (Guadeloupe, French West Indies). *Geosphere*, 15(4), 983–1007.
- Leonard, N. D., Welsh, K. J., Zhao, J., Nothdurft, L. D., Webb, G. E., Major, J., et al. (2013). Mid-holocene sea-level and coral reef demise: U-Th dating of subfossil corals in Moreton Bay, Australia. *The Holocene*, 23(12), 1841–1852.

- Lin, J.-Y., Sibuet, J.-C., Hsu, S.-K., & Wu, W.-N. (2014). Could a Sumatra-like megathrust earthquake occur in the south Ryukyu subduction zone? *Earth Planets and Space*, 66(1), 49.
- Mallick, R., Meltzner, A. J., Tsang, L. L. H., Lindsey, E. O., Feng, L., & Hill, E. M. (2021). Long-lived shallow slow-slip events on the Sunda megathrust. *Nature Geoscience*, 14(5), 327–333.
- Matsumoto, T., Shinjo, R., Nakamura, M., Kimura, M., & Ono, T. (2009). Submarine active normal faults completely crossing the southwest Ryukyu Arc. *Tectonophysics*, 466(3), 289–299.
- Meltzner, A. J., Sieh, K., Abrams, M., Agnew, D. C., Hudnut, K. W., Avouac, J.-P., & Natawidjaja, D. H. (2006). Uplift and subsidence associated with the great Aceh-Andaman earthquake of 2004. *Journal of Geophysical Research*, 111(B2), B02407.
- Meltzner, A. J., Sieh, K., Chiang, H.-W., Shen, C.-C., Suwargadi, B. W., Natawidjaja, D. H., et al. (2010). Coral evidence for earthquake recurrence and an A.D. 1390–1455 cluster at the south end of the 2004 Aceh–Andaman rupture. *Journal of Geophysical Research*, 115(B10), B10402.
- Meltzner, A. J., Sieh, K., Chiang, H.-W., Wu, C.-C., Tsang, L. L. H., Shen, C.-C., et al. (2015). Time-varying interseismic strain rates and similar seismic ruptures on the Nias–Simeulue patch of the Sunda megathrust. *Quaternary Science Reviews*, 122, 258–281.
- Meltzner, A. J., Switzer, A. D., Horton, B. P., Ashe, E., Qiu, Q., Hill, D. F., et al. (2017). Half-metre sea-level fluctuations on centennial timescales from mid-Holocene corals of Southeast Asia. *Nature Communications*, 8(1), 14387.
- Meltzner, A. J., & Woodroffe, C. D. (2015). Coral microatolls. *Handbook of Sea-Level Research*, 125–145.
- Meysignac, B., & Cazenave, A. (2012). Sea level: A review of present-day and recent-past changes and variability. *Journal of Geodynamics*, 58, 96–109.
- Meysignac, B., Salas y Melia, D., Becker, M., Llovel, W., & Cazenave, A. (2012). Tropical Pacific spatial trend patterns in observed sea level: Internal variability and/or anthropogenic signature? *Climate of the Past*, 8(2), 787–802.
- Minami, H., & Ohara, Y. (2018). Detailed volcanic morphology of Daisan-Miyako Knoll in the southern Ryukyu arc. *Marine Geology*, 404, 97–110.
- Mouslopoulou, V., Oncken, O., Hainzl, S., & Nicol, A. (2016). Uplift rate transients at subduction margins due to earthquake clustering. *Tectonics*, 35(10), 2370–2384.
- Nakamura, M. (2006). Source Fault model of the 1771 Yaeyama tsunami, southern Ryukyu Islands, Japan, inferred from numerical simulation. *Pure and Applied Geophysics*, 163(1), 41–54.
- Nakamura, M. (2009). Fault model of the 1771 Yaeyama earthquake along the Ryukyu Trench estimated from the devastating tsunami. *Geophysical Research Letters*, 36(19), L19307.
- Nakamura, M. (2017). Distribution of low-frequency earthquakes accompanying the very low frequency earthquakes along the Ryukyu Trench. *Earth Planets and Space*, 69(1), 49.
- Nakamura, M., & Sunagawa, N. (2015). Activation of very low frequency earthquakes by slow slip events in the Ryukyu Trench. *Geophysical Research Letters*, 42(4), 1076–1082.
- Nakata, T., & Kawana, T. (1995). Historical and prehistorical large tsunamis in the southern Ryukyus, Japan. In Y. Tsuchiya & N. Shuto (Eds.), (Eds.), *Tsunami: Progress in prediction, disaster prevention and warning* (pp. 211–221). Springer Netherlands.
- Natawidjaja, D. H., Sieh, K., Chlieh, M., Galetzka, J., Suwargadi, B. W., Cheng, H., et al. (2006). Source parameters of the great Sumatran megathrust earthquakes of 1797 and 1833 inferred from coral microatolls. *Journal of Geophysical Research*, 111(B6), 37.
- Natawidjaja, D. H., Sieh, K., Ward, S. N., Cheng, H., Edwards, R. L., Galetzka, J., & Suwargadi, B. W. (2004). Paleogeodetic records of seismic and aseismic subduction from central Sumatran microatolls, Indonesia. *Journal of Geophysical Research*, 109(B4), B04306.
- Nishimura, S., Hashimoto, M., & Ando, M. (2004). A rigid block rotation model for the GPS derived velocity field along the Ryukyu arc. *Physics of the Earth and Planetary Interiors*, 142(3–4), 185–203.
- Nishimura, T. (2014). Short-term slow slip events along the Ryukyu Trench, southwestern Japan, observed by continuous GNSS. *Progress in Earth and Planetary Science*, 1(1), 22.
- Nishizawa, A., Kaneda, K., Oikawa, M., Horiuchi, D., Fujioka, Y., & Okada, C. (2017). Variations in seismic velocity distribution along the Ryukyu (Nansei-Shoto) Trench subduction zone at the northwestern end of the Philippine Sea plate. *Earth Planets and Space*, 69(1), 86.
- Obara, K., & Kato, A. (2016). Connecting slow earthquakes to huge earthquakes. *Science*, 353(6296), 253–257.
- Okada, Y. (1992). Internal deformation due to shear and tensile faults in a half-space. *Bulletin of the Seismological Society of America*, 82(2), 1018–1040.
- Okamoto, M., Nojima, S., & Furushima, Y. (2007). Temperature environments during coral bleaching events in Sekisei lagoon [Japan]. *Bulletin of the Japanese Society of Fisheries Oceanography (Japan)*.
- Okamura, Y., Nishizawa, A., Fujii, Y., & Yanagisawa, H. (2018). Accretionary prism collapse: A new hypothesis on the source of the 1771 giant tsunami in the Ryukyu Arc, SW Japan. *Scientific Reports*, 8(1), 13620.
- Okamura, Y., Nishizawa, A., Oikawa, M., & Horiuchi, D. (2017). Differential subsidence of the forearc wedge of the Ryukyu (Nansei-Shoto) Arc caused by subduction of ridges on the Philippine Sea Plate. *Tectonophysics*, 717, 399–412.
- Otsubo, M., & Hayashi, D. (2003). Neotectonics in Southern Ryukyu arc by means of paleostress analysis. *Bulletin-Faculty of Science University of The Ryukyus*, (76), 1–74.
- Ozawa, S., Nishimura, T., Munekane, H., Suito, H., Kobayashi, T., Tobita, M., & Imakiire, T. (2012). Preceding, coseismic, and postseismic slips of the 2011 Tohoku earthquake, Japan. *Journal of Geophysical Research*, 117(B7), B07404.
- Peña, C., Heidebach, O., Moreno, M., Bedford, J., Ziegler, M., Tassara, A., & Oncken, O. (2020). Impact of power-law rheology on the viscoelastic relaxation pattern and afterslip distribution following the 2010 M_w 8.8 Maule earthquake. *Earth and Planetary Science Letters*, 542, 116292.
- Peterson, E. T., & Seno, T. (1984). Factors affecting seismic moment release rates in subduction zones. *Journal of Geophysical Research*, 89(B12), 10233–10248.
- Philibosian, B., Feuillet, N., Weil-Accardo, J., Jacques, E., Guihou, A., Mériaux, A.-S., et al. (2022). 20th-century strain accumulation on the Lesser Antilles megathrust based on coral microatolls. *Earth and Planetary Science Letters*, 579, 117343.
- Philibosian, B., Sieh, K., Avouac, J. P., Natawidjaja, D. H., Chiang, H. W., Wu, C. C., et al. (2014). Rupture and variable coupling behavior of the Mentawai segment of the Sunda megathrust during the supercycle culmination of 1797 to 1833. *Journal of Geophysical Research: Solid Earth*, 119(9), 7258–7287.
- Philibosian, B., Sieh, K., Avouac, J.-P., Natawidjaja, D. H., Chiang, H.-W., Wu, C.-C., et al. (2017). Earthquake supercycles on the Mentawai segment of the Sunda megathrust in the seventeenth century and earlier. *Journal of Geophysical Research: Solid Earth*, 122(1), 642–676.
- Philibosian, B., Sieh, K., Natawidjaja, D. H., Chiang, H.-W., Shen, C.-C., Suwargadi, B. W., et al. (2012). An ancient shallow slip event on the Mentawai segment of the Sunda megathrust, Sumatra. *Journal of Geophysical Research*, 117(B5), B05401.
- Reid, C., Begg, J., Mouslopoulou, V., Oncken, O., Nicol, A., & Kufner, S. K. (2020). Using a calibrated upper living position of marine biota to calculate coseismic uplift: A case study of the 2016 Kaikōura earthquake, New Zealand. *Earth Surface Dynamics*, 8(2), 351–366.

- Report of the coordinating Committee for Earthquake Prediction, Japan. (1993) Report, Vol.49. (s. d.). Retrieved from <https://cais.gsi.go.jp/YOCHIREN/report/index49.e.html>
- Rosenfeld, M., Shemesh, A., Yam, R., Sakai, K., & Loya, Y. (2006). Impact of the 1998 bleaching event on $\delta^{18}\text{O}$ records of Okinawa corals. *Marine Ecology Progress Series*, 314, 127–133.
- Ruiz, S., Metois, M., Fuenzalida, A., Ruiz, J., Leyton, F., Grandin, R., et al. (2014). Intense foreshocks and a slow slip event preceded the 2014 Iquique M_w 8.1 earthquake. *Science*, 345(6201), 1165–1169.
- Savage, J. C. (1983). A dislocation model of strain accumulation and release at a subduction zone. *Journal of Geophysical Research*, 88(B6), 4984–4996.
- Scholz, C. H., & Campos, J. (2012). The seismic coupling of subduction zones revisited. *Journal of Geophysical Research*, 117(B5), B05310.
- Scoffin, T. P., Stoddart, D. R., Rosen, B. R., Stoddart, D. R., & Yonge, M. (1978). The nature and significance of microatolls. *Philosophical Transactions of the Royal Society of London B Biological Sciences*, 284(999), 99–122.
- Shelly, D. R., Beroza, G. C., & Ide, S. (2007). Non-volcanic tremor and low-frequency earthquake swarms. *Nature*, 446(7133), 305–307.
- Shen, C.-C., Li, K.-S., Sieh, K., Natawidjaja, D., Cheng, H., Wang, X., et al. (2008). Variation of initial $^{230}\text{Th}/^{232}\text{Th}$ and limits of high precision U–Th dating of shallow-water corals. *Geochimica et Cosmochimica Acta*, 72(17), 4201–4223.
- Shimazaki, K., & Nakata, T. (1980). Time-predictable recurrence model for large earthquakes. *Geophysical Research Letters*, 7(4), 279–282.
- Shiono, K., Mikumo, T., & Ishikawa, Y. (1980). Tectonics of the Kyushu-Ryukyu Arc as evidenced from seismicity and focal mechanism of shallow to intermediate-depth earthquakes. *Journal of Physics of the Earth*, 28(1), 17–43.
- Shyu, J. B. H., Wang, C.-C., Wang, Y., Shen, C.-C., Chiang, H.-W., Liu, S.-C., et al. (2018). Upper-plate splay fault earthquakes along the Arakan subduction belt recorded by uplifted coral microatolls on northern Ramree Island, western Myanmar (Burma). *Earth and Planetary Science Letters*, 484, 241–252.
- Sibuet, J.-C., Deffontaines, B., Hsu, S.-K., Thareau, N., Le Formal, J.-P., & Liu, C.-S. (1998). Okinawa trough backarc basin: Early tectonic and magmatic evolution. *Journal of Geophysical Research*, 103(B12), 30245–30267.
- Sibuet, J.-C., Letouzey, J., Barbier, F., Charvet, J., Foucher, J.-P., Hilde, T. W. C., et al. (1987). Back Arc extension in the Okinawa Trough. *Journal of Geophysical Research*, 92(B13), 14041–14063.
- Sieh, K., Natawidjaja, D. H., Meltzner, A. J., Shen, C. C., Cheng, H., Li, K. S., et al. (2008). Earthquake supercycles inferred from sea-level changes recorded in the corals of west Sumatra. *Science*, 322(5908), 1674–1678.
- Smithers, S., & Hopley, D. (2011). *Coral cay classification and evolution*. In D. Hopley, (Ed.), (pp. 237–254). Springer.
- Song, S., Peng, Z., Zhou, W., Liu, W., Liu, Y., & Chen, T. (2012). Variation of the winter monsoon in South China Sea over the past 183 years: Evidence from oxygen isotopes in coral. *Global and Planetary Change*, 98–99, 131–138.
- Sowa, K., Watanabe, T., Kan, H., & Yamano, H. (2014). Influence of land development on Holocene porites coral calcification at Nagura Bay, Ishigaki Island, Japan. *PLoS One*, 9(2), e88790.
- Stoddart, D. R., & Scoffin, T. P. (1979). Microatolls: Review of form, origin and terminology. *Atoll Research Bulletin*, 224, 1–17.
- Suzuki, A., Gagan, M. K., Fabricius, K., Isdale, P. J., Yukino, I., & Kawahata, H. (2003). Skeletal isotope microprofiles of growth perturbations in Porites corals during the 1997–1998 mass bleaching event. *Coral Reefs*, 22(4), 357–369.
- Suzuki, A., Yokoyama, Y., Kan, H., Minoshima, K., Matsuzaki, H., Hamanaka, N., & Kawahata, H. (2008). Identification of 1771 Meiwu Tsunami deposits using a combination of radiocarbon dating and oxygen isotope microprofiling of emerged massive Porites boulders. *Quaternary Geochronology*, 3(3), 226–234.
- Tadokoro, K., Nakamura, M., Ando, M., Kimura, H., Watanabe, T., & Matsuhiro, K. (2018). Interplate coupling state at the Nansei-Shoto (Ryukyu) trench, Japan, deduced from seafloor crustal deformation measurements. *Geophysical Research Letters*, 45(14), 6869–6877.
- Takagi, R., Uchida, N., & Obara, K. (2019). Along-strike variation and migration of long-term slow slip events in the western Nankai subduction zone, Japan. *Journal of Geophysical Research: Solid Earth*, 124(4), 3853–3880.
- Taylor, F. W., Briggs, R. W., Frohlich, C., Brown, A., Hornbach, M., Papabatu, A. K., et al. (2008). Rupture across arc segment and plate boundaries in the 1 April 2007 Solomons earthquake. *Nature Geoscience*, 1(4), 253–257.
- Taylor, F. W., Frohlich, C., Lecolle, J., & Strecker, M. (1987). Analysis of partially emerged corals and reef terraces in the central Vanuatu Arc: Comparison of contemporary coseismic and nonseismic with Quaternary vertical movements. *Journal of Geophysical Research*, 92(B6), 4905–4933.
- Taylor, F. W., Isacks, B. L., Jouannic, C., Bloom, A. L., & Dubois, J. (1980). Coseismic and quaternary vertical tectonic movements, Santo and Malekula Islands, New Hebrides Island Arc. *Journal of Geophysical Research*, 85(B10), 5367–5381.
- Taylor, F. W., Jouannic, C., Gilpin, L., & Bloom, A. (1982). Coral colonies as monitors of change in relative level of the land and sea: Applications to vertical tectonism. In *Proceedings of 4th international coral reef congress*, (pp. 485–492).
- Taylor, F. W., Mann, P., Bevis, M. G., Edwards, R. L., Cheng, H., Cutler, K. B., et al. (2005). Rapid forearc uplift and subsidence caused by impinging bathymetric features: Examples from the New Hebrides and Solomon arcs. *Tectonics*, 24(6).
- Tozer, B., Sandwell, D. T., Smith, W. H., Olson, C., Beale, J. R., & Wessel, P. (2019). Global bathymetry and topography at 15 arc sec: SRTM15+. *Earth and Space Science*, 6(10), 1847–1864.
- Tsuji, Y. (1993). Tide influenced high energy environments and rhodolith-associated carbonate deposition on the outer shelf and slope off the Miyako Islands, southern Ryukyu Island Arc, Japan. *Marine Geology*, 113(3), 255–271.
- Tsuji, Y. (1997). Damage to villages on Amami archipelago due to the 1995 Amami-Oshima-Kinkai earthquake-tsunami. *Journal of Geography*, 106(4), 486–502.
- Vigny, C., Socquet, A., Peyrat, S., Ruegg, J. C., Métois, M., Madariaga, R., et al. (2011). The 2010 M_w 8.8 Maule megathrust earthquake of central Chile, monitored by GPS. *Science*, 332(6036), 1417–1421.
- Wan, J. X. W., Meltzner, A. J., Switzer, A. D., Lin, K., Wang, X., Bradley, S. L., et al. (2020). Relative sea-level stability and the radiocarbon marine reservoir correction at Natuna Island, Indonesia, since 6400 yr BP. *Marine Geology*, 430, 106342.
- Wang, Y., Shyu, J. B. H., Sieh, K., Chiang, H.-W., Wang, C.-C., Aung, T., et al. (2013). Permanent upper plate deformation in western Myanmar during the great 1762 earthquake: Implications for neotectonic behavior of the northern Sunda megathrust. *Journal of Geophysical Research: Solid Earth*, 118(3), 1277–1303.
- Watanabe, T., & Tabei, T. (2004). GPS velocity field and seismotectonics of the Ryukyu arc, southwest Japan. *Jishin*, 57(1), 1–10.
- Wei, D., & Seno, T. (1998). Determination of the Amurian plate motion. In *Mantle dynamics and plate interactions in East Asia* (pp. 337–346). American Geophysical Union (AGU).
- Weil-Accardo, J. (2014). *Paléosismicité, cycle sismique et couplage tectonique de la subduction antillaise par l'étude des microatolls coralliens et des terrasses marines* (Ph. D. dissertation). Paris Diderot University, Institut de Physique du Globe de Paris.

- Weil-Accardo, J., Feuillet, N., Jacques, E., Deschamps, P., Beauducel, F., Cabioch, G., et al. (2016). Two hundred thirty years of relative sea level changes due to climate and megathrust tectonics recorded in coral microatolls of Martinique (French West Indies). *Journal of Geophysical Research: Solid Earth*, *121*(4), 2873–2903.
- Weil-Accardo, J., Feuillet, N., Jacques, E., Deschamps, P., Saurel, J.-M., Thirumalai, K., et al. (2016). Relative sea-level changes during the last century recorded by coral microatolls in Belloc, Haiti. *Global and Planetary Change*, *139*, 1–14.
- Weil-Accardo, J., Feuillet, N., Satake, K., Goto, T., Goto, K., Harada, T., et al. (2020). Relative Sea-level changes over the past centuries in the central Ryukyu Arc inferred from coral microatolls. *Journal of Geophysical Research: Solid Earth*, *125*(2), e2019JB018466.
- Woodroffe, C., & McLean, R. (1990). Microatolls and recent sea level change on coral atolls. *Nature*, *344*(6266), 531–534.
- Woodroffe, C. D., McGregor, H. V., Lambeck, K., Smithers, S. G., & Fink, D. (2012). Mid-Pacific microatolls record sea-level stability over the past 5000 yr. *Geology*, *40*(10), 951–954.
- Yamaguchi, T. (2016). A review of coral studies of the Ryukyu Island Arc to reconstruct its long-term landscape history. In H. Kayanne (Ed.), (Ed.), *Coral reef science: Strategy for ecosystem symbiosis and coexistence with humans under multiple stresses* (pp. 55–63). Springer Japan.
- Yamano, H., Inoue, T., Adachi, H., Tsukaya, K., Adachi, R., & Baba, S. (2019). Holocene sea-level change and evolution of a mixed coral reef and mangrove system at Iriomote Island, southwest Japan. *Estuarine, Coastal and Shelf Science*, *220*, 166–175.
- Yu, K.-F., Zhao, J.-X., Done, T., & Chen, T.-G. (2009). Microatoll record for large century-scale sea-level fluctuations in the mid-Holocene. *Quaternary Research*, *71*(3), 354–360.
- Zachariasen, J., Sieh, K., Taylor, F. W., Edwards, R. L., & Hantoro, W. S. (1999). Submergence and uplift associated with the giant 1833 Sumatran subduction earthquake: Evidence from coral microatolls. *Journal of Geophysical Research*, *104*(B1), 895–919.
- Zachariasen, J., Sieh, K., Taylor, F. W., & Hantoro, W. S. (2000). Modern vertical deformation above the Sumatran subduction zone: Paleogeodetic insights from coral microatolls. *Bulletin of the Seismological Society of America*, *90*(4), 897–913.
- Zachariasen, J. A. (1998). *Paleoseismology and paleogeodesy of the Sumatran subduction zone: A study of vertical deformation using coral microatolls* (Ph D. Thesis). California Institute of Technology.

References From the Supporting Information

- Fujita, K., Shimoji, H., & Nagai, K. (2006). Paleoenvironmental interpretations of Quaternary reef deposits based on comparisons of 10 selected modern and fossil larger foraminifera from the Ryukyu Islands, Japan. *Island Arc*, *15*(4), 420–436.
- Kawana, T., & Pirazzoli, P. A. (1990). Re-Examination on the Holocene emerged shorelines in Iribu and Shimoji Islands, the South Ryukyus, Japan. *The Quaternary Research (Daiyonki-Kenkyu)*, *28*(5), 419–426.